From Femtoseconds to Gigaseconds: The SolDeg Project to Analyze Heterojunction and TOPCon Cell Degradation with Machine Learning

1. Degradation in Si-only heterojunctions

2. Development of a Machine-Learning trained Si-H interatomic potential

3. Experimental HJ degradation study

4. Degradation in c-Si/a-Si:H heterojunctions

5. Degradation in TOPCon cells

Andrew Diggs (UCD)
Zitong Zhao (UCD)
Adam Goga (UCD)
Zachary Crawford (UCD)
Davis Unruh (UCD-Samsung)
Reza Vatan (ASU-First Solar)
Salman Manzoor (ASU-First Solar)
Mariana Bertoni (ASU)
Stephen Goodnick (ASU)
Gabor Csanyi (Cambridge, UK)
Gergely Zimanyi (UCD)

Supported by DOE SETO

I Love Switzerland

Aareschlucht

Lucerne

ITPRV: The two leading designs of the next generation: HJ and TOPCon

2023 edition of

Today PERC dominates

By early 2030s, the share of TOPCon will reach 60%, and Heterojunction 20%
What factors will impact the relative acceptance of these leading designs:
- Efficiency
- Type of wafer
- Silver needs

We wish to assist this decision by shining the light on one more factor:
Degradation rates, mitigation possibilities

High HJ Degradation rates were reported

* Si Heterojunction cells hold Si world record efficiency of 26.7%
* Si HJ cells are a leading candidate for tandem bottom cells
* Efficiency degradation rates of 1%/yr were reported, twice the usual. The extra 0.5%/yr degradation was attributed to Voc
* Eliminating this 0.5%/yr degradation would have the effect of increasing the efficiency by close to 1.5-2% in terms of LCOE, based on the System Advisor Model

Possible driver?
Defects at interface!
Bertoni Phys. Stat. Sol. 2018

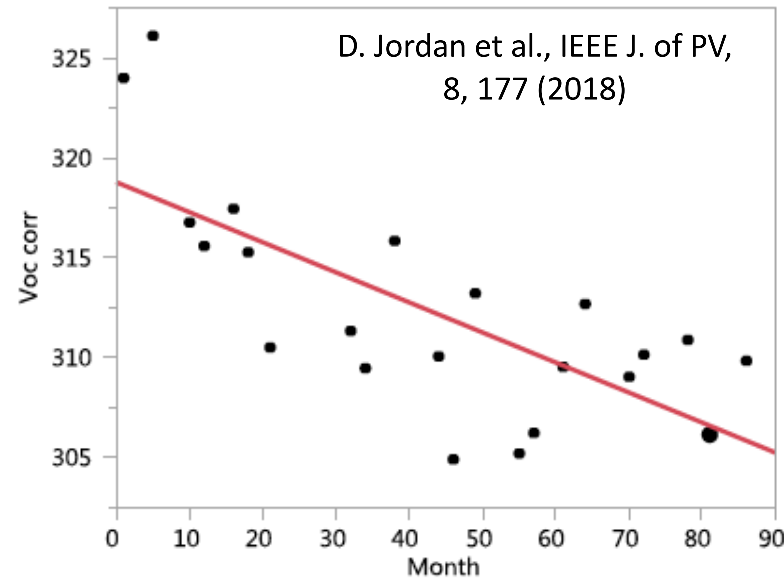

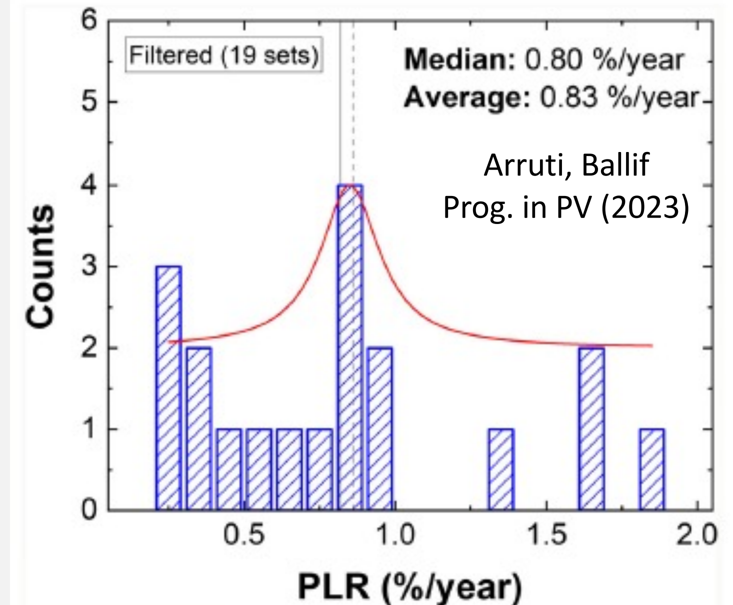

1. The SolDeg platform

We developed the SolDeg platform to analyze the formation of defects at the c-Si/a-Si interface
This requires

1. Connecting extreme time scales from femtoseconds to gigaseconds (30 years)

2. Simulation of large number of large samples with extreme precision

Si-only HJs

1. Create c-Si/a-Si stacks

2. Generate blasted clusters at the c-Si/a-Si interface as likely hosts of electronic defects

3. Identify blasted clusters that actually host electronic defects

4. Determine the energy barriers that control the generation of these electronic defects

5. Determine the distribution of these barriers

6. Determine the defect generation dynamics from the energy barrier distribution

Si-only HJs: Precise structures by Machine Learning-trained Potentials

1. Create c-Si/a-Si stacks using Molecular Dynamics with Machine-Learning (ML)-developed Si-Si potential: Gaussian Approximation Potential Si GAP. -- Timestep: femtoseconds

GAP reproduces DFT much better than other interatomic potentials.

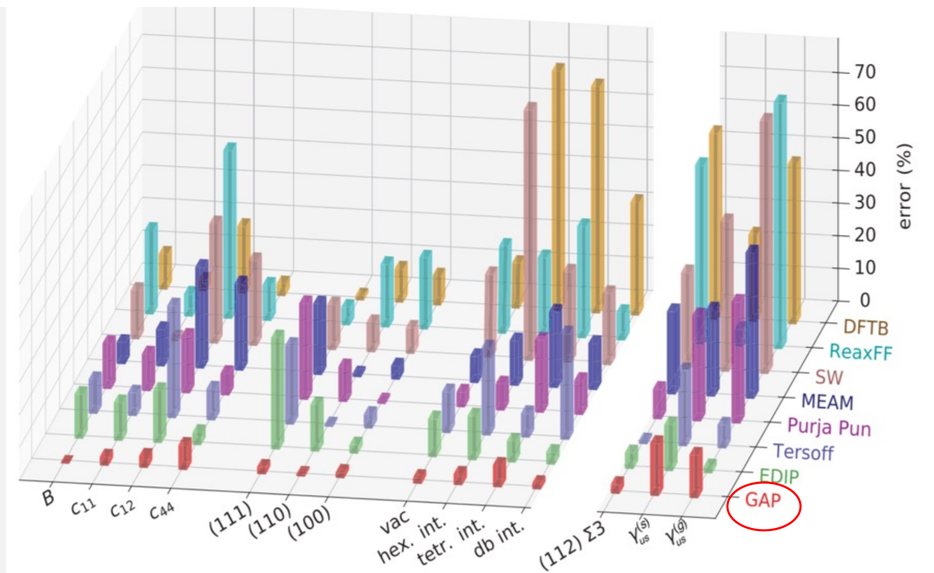

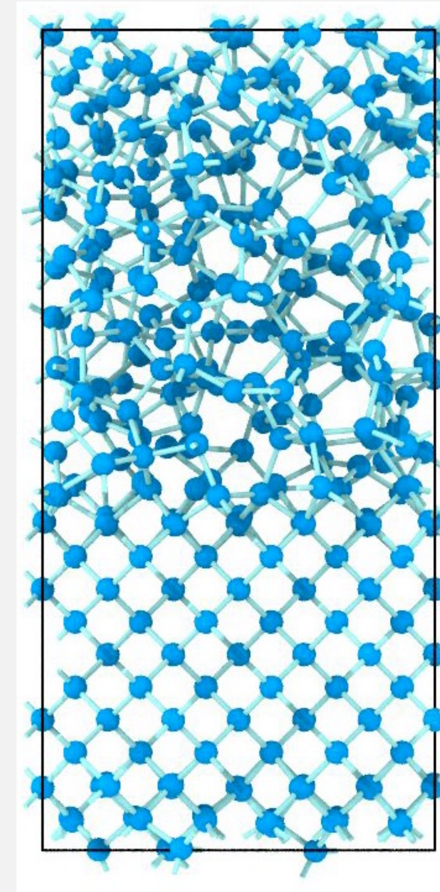

Creating Structural Defects and Identifying Electronic Defects

2. Generate shocked clusters at the c-Si/a-Si interface with "cluster-blaster" as likely hosts of electronic defects
We created 1,500 blasted clusters

3. Identify shocked clusters that actually host electronic defects: Inverse Participation Ratio (IPR) method. 500 of the clusters supported electronic defects.

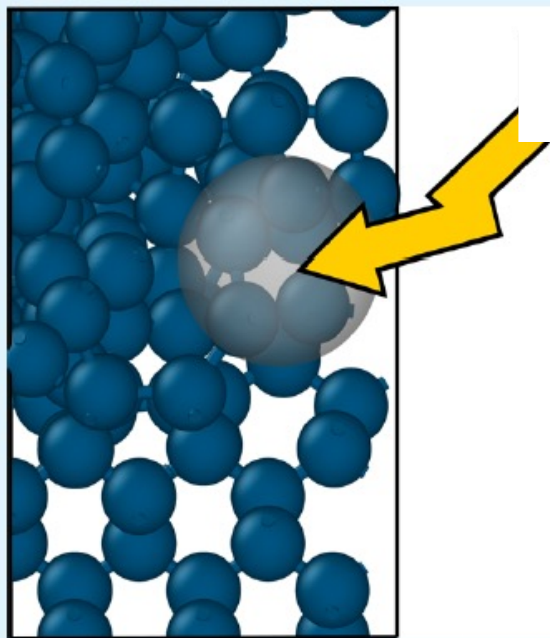

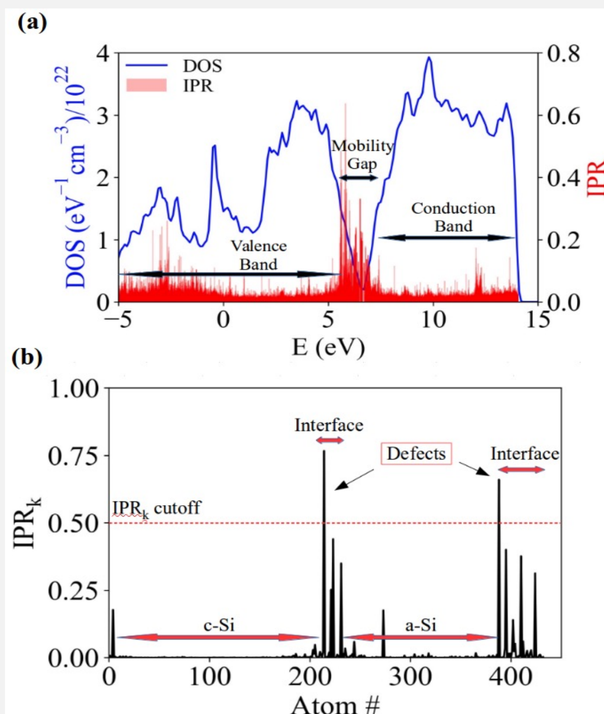

Connect Decades of Time Scales: Nudged Elastic Band Method

4. Determine energy barriers that control the generation of the electronic defects:

Nudged Elastic Band method

Start with a path that connects initial and final state over barrier, then nudge it. The relaxing band finds lowest energy barrier/saddlepoint.

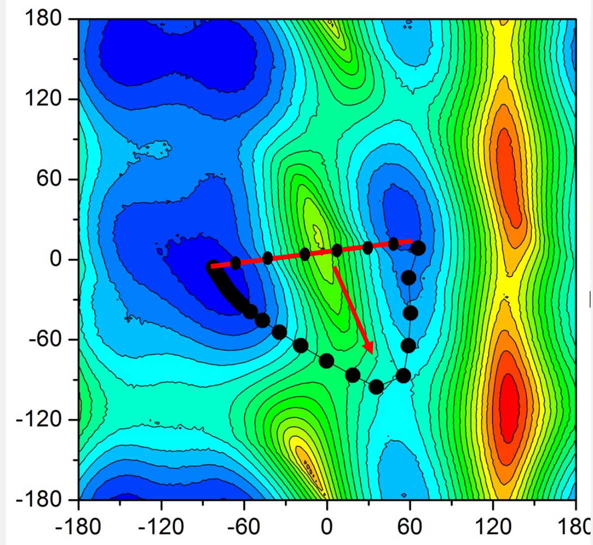

5. Determine the barrier distribution for 500 barriers

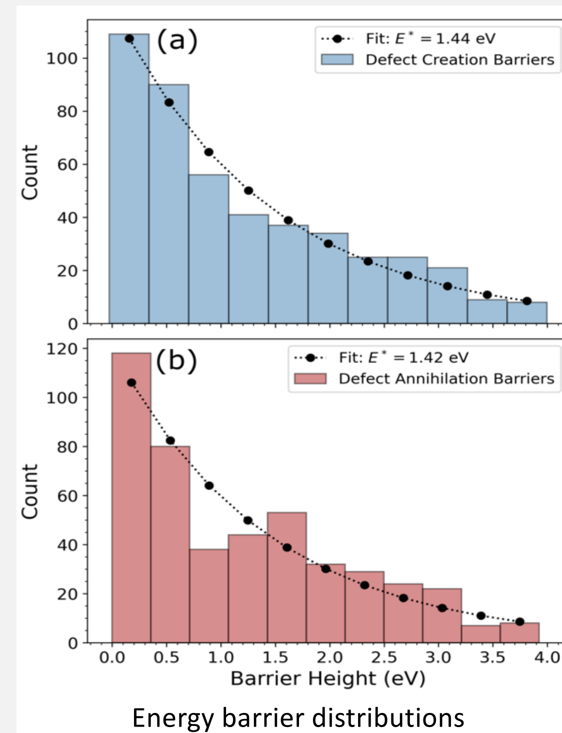

Energy barrier distributions

Determine and Analyze Dynamics of Defect Generation

6. Use Kinetic Monte Carlo dynamics of thermally activated processes over barriers.

But simulation gets stuck in deep valleys. We accelerated simulation:

- Identify deep valleys (superbasins)
- Accelerate break out from valleys

Accelerated Superbasin Kinetic Monte Carlo

Integrate out fast degrees of freedom as in Renorm Group

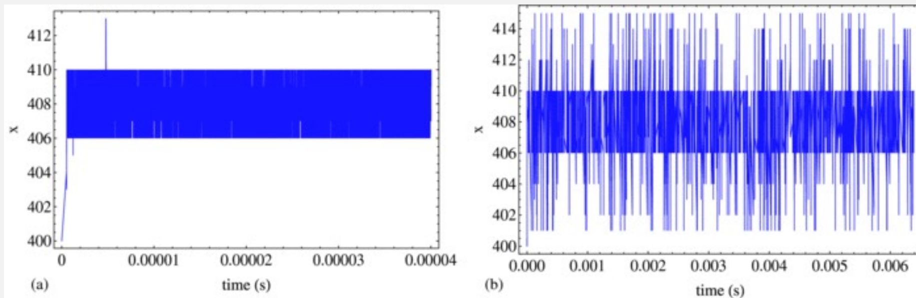

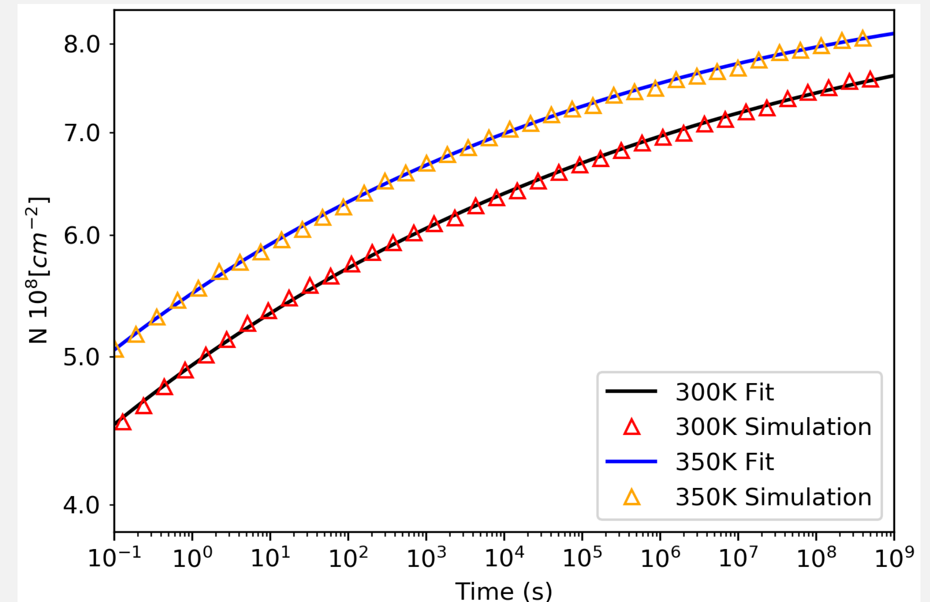

τ_0(ps) exp $^{(1.3\text{eV}/300\text{K})}$ ~ 10^9sec (gigasec)=30 years

$$N(t) = N_{sat}(1 - \exp[-(t/\tau_0)^{\beta}])$$

β =kT/E*

Data are well fitted by stretched exponential

Why? Because P(E) can be fitted by P(E)~exp(-E/E*)

Time Correspondence Curve for Accelerated Testing

Accelerated testing at elevated temperature:
Construct Time correspondence curve
N(T=350K,tacc)=N(T=300K,tnorm)

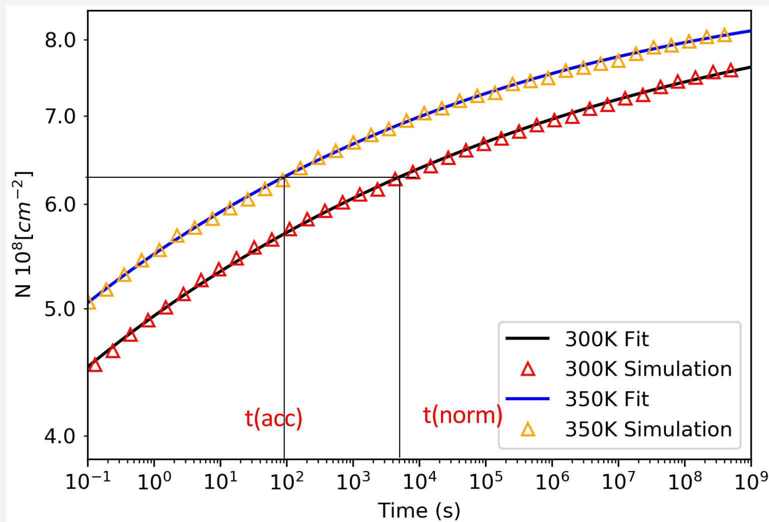

Stretched exponential analytically predicts:
$t(norm) \sim t(acc)^{(T(acc)/T(norm))}$
350K/300K=1.17

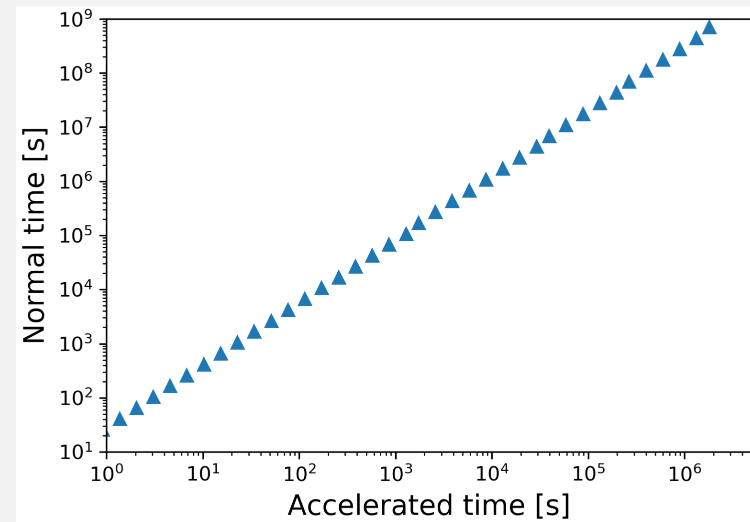

Fitting the simulation: $t(norm) \sim t(acc)^s$
s = 1.17

2. SolDeg for c-Si/a-Si:H: Needed: Machine-Learning trained Si-H GAP

Problem: no Machine Learning-based Si-H (GAP) potential
We developed the world's first Si-H Machine Learning-trained GAP potential that delivers the highest precision

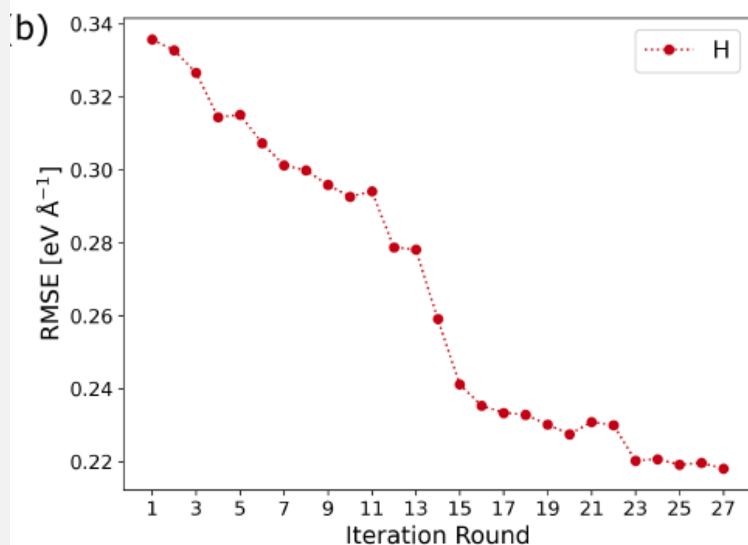

Forces: Deviation from DFT
substantially reduced

Iteration	Structure Type
1	Optimized structures (all phases)
2	Optimized structures (all phases)
3	Low T anneal of a-Si:H
4	High T anneal of liq-Si:H
5	High T anneal of liq-Si:H
6	Med T anneal (1100K) of a-Si:H
7	Heating a-Si:H from 500K to 800K at 10^{13} K/s
8	Heating a-Si:H from 800K to 1100K at 10^{13} K/s
9	Heating a-Si:H from 1100K to 1400K at 10^{13} K/s
10	Heating a-Si:H from 1100K to 1400K at 10^{13} K/s
11	Heating a-Si:H from 800K to 1400K at 10^{12} K/s
12	Added new a-Si:H structures
13	Add new a-Si:H structures
14	Added c-Si/a-Si:H interface structures
15	Added c-Si/a-Si:H interface structures
16	Added new c-Si divacancy structures
17	Added new liq-Si:H structures
18	Added new c-Si vacancy structures
19	Added new c-Si interstitial structures
20	Low T anneal of c-Si/a-Si:H interface structures
21	Optimization of c-Si/a-Si:H interface structures
22	NPT high T anneal of liq-Si:H structures
23	NVT high T anneal of liq-Si:H structures
24	Quenching liq-Si:H from 2000K to 1500K at 10^{13} K/s
25	Annealing quenched liq-Si:H structures at 1500K
26	Quenching liq-Si:H from 1500K to 1400K at 10^{12} K/s
27	Added hydrogen passivated c-Si surface (100) and c-Si surface (111) structures

27 Rounds of ML-training Created Precise, Efficient Si-H GAP

1. Energies: reproduces DFT within 4 meV/atom

2. Accuracy of reproducing DFT forces improved by 35%.

3. Radial correlation function

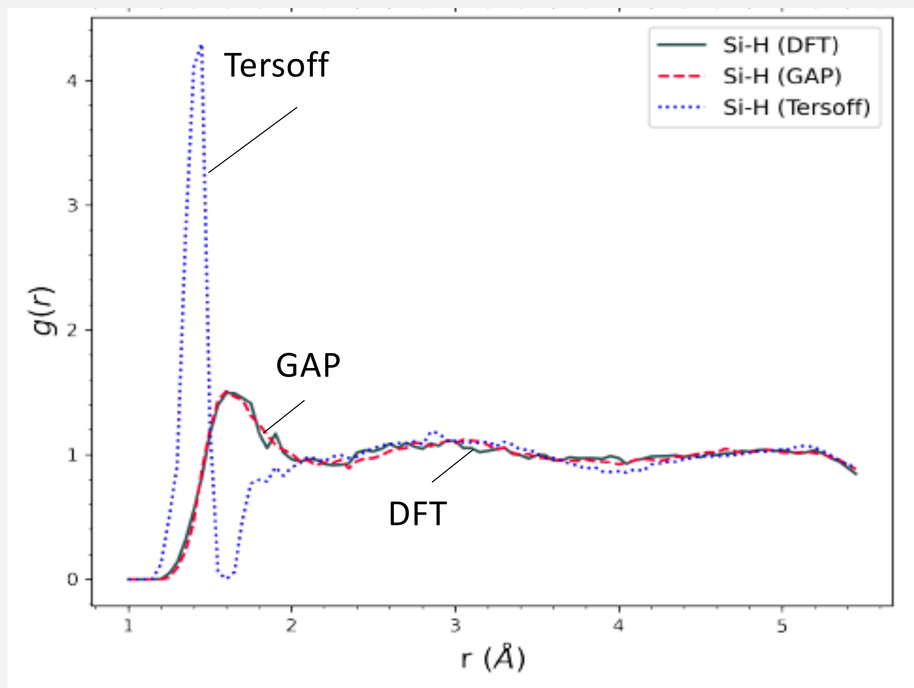

4. Bond angle distribution function

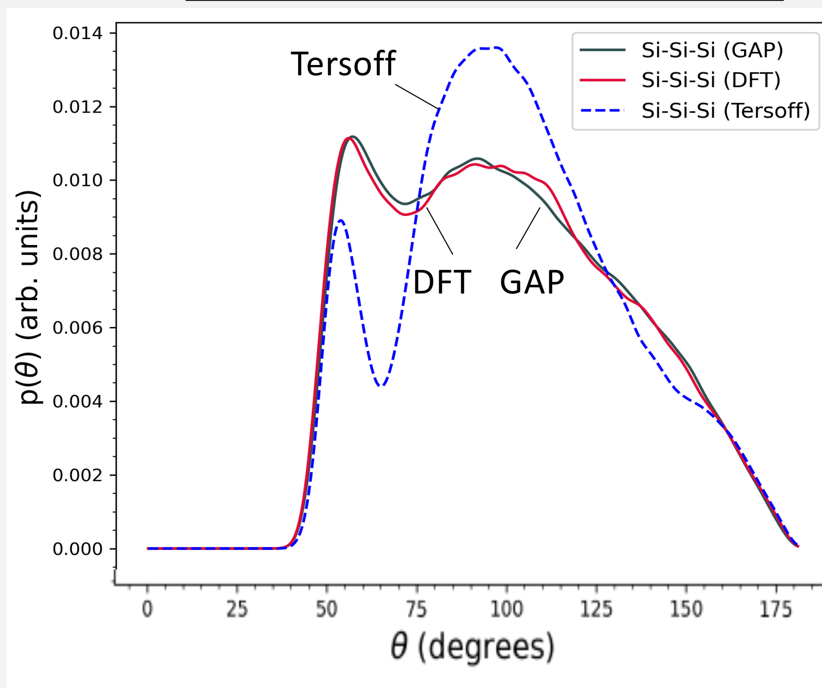

Si-H GAP: Reaching the unreachable in size and precision

Run time scaling: GAP O(N); DFT O(N^3)
DFT can simulate 400-500 atoms
Si:H GAP simulation: 4,096 Si and 558 H atoms

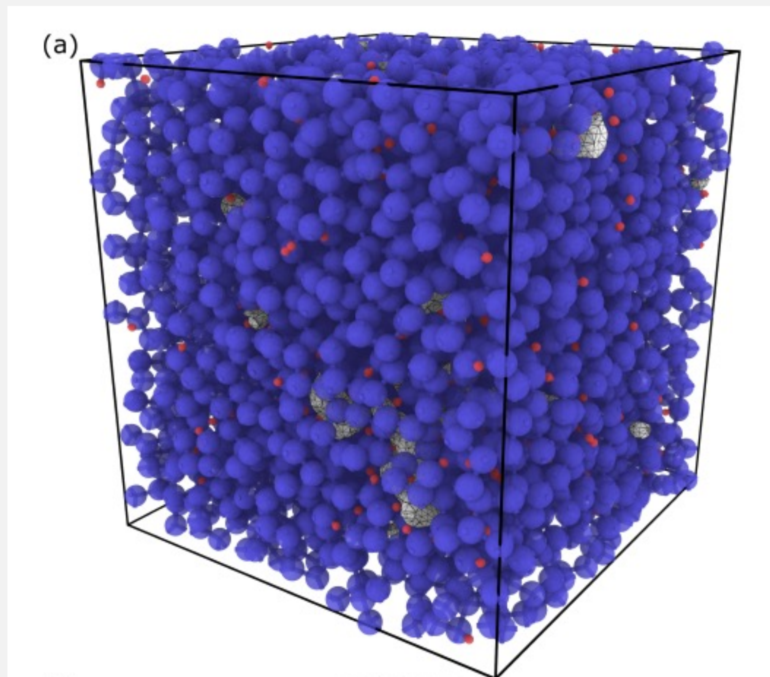

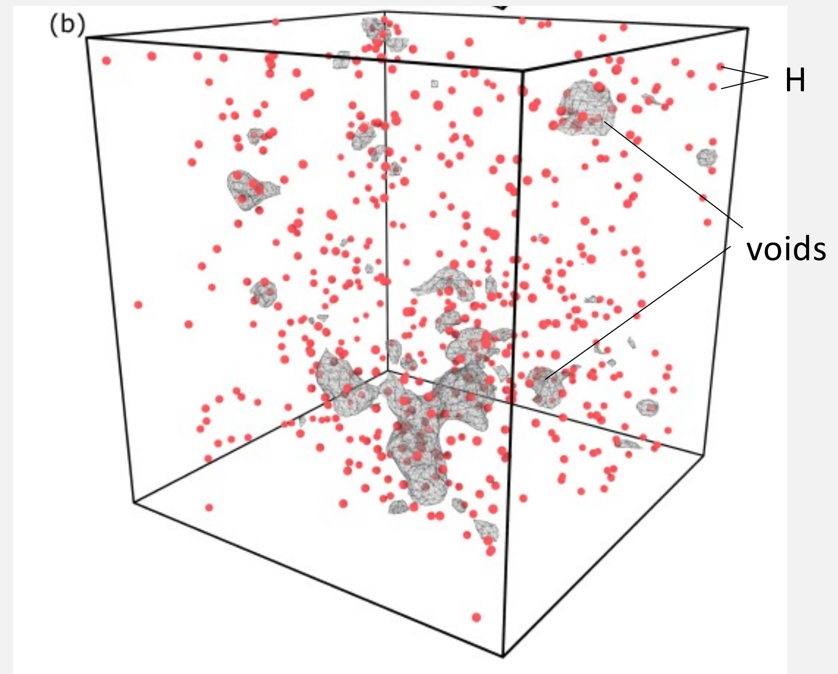

Si:H GAP Molecular Dynamics simulations can reach unparalleled sizes and number of realizations

3. Experimental analysis of SHJ degradation: Samples, Stressors

Bertoni, Manzoor (ASU)

Samples

a-Si:H(i) ~50 nm
c-Si (160-270 µm)
a-Si:H(i) ~50 nm

Deposition Conditions

Name	Value
Frequency	13.56 MHz
Pressure	3.2 Torr
Power	200 W
H_2	200 sccm
SiH_4	40 sccm
Temperature	220 °C
Deposition rate	0.5 nm/sec

Characterization

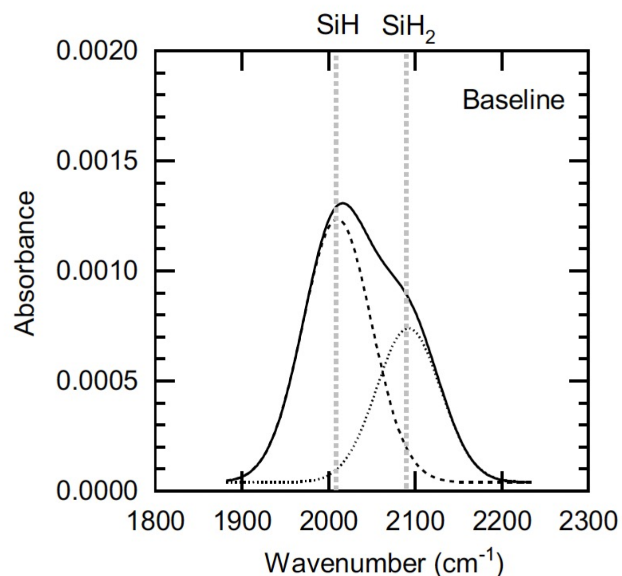

Bandgap	H conc.	ρ (g/cm³)	E_u (meV)
1.68 eV	15 at.%	2.25	48

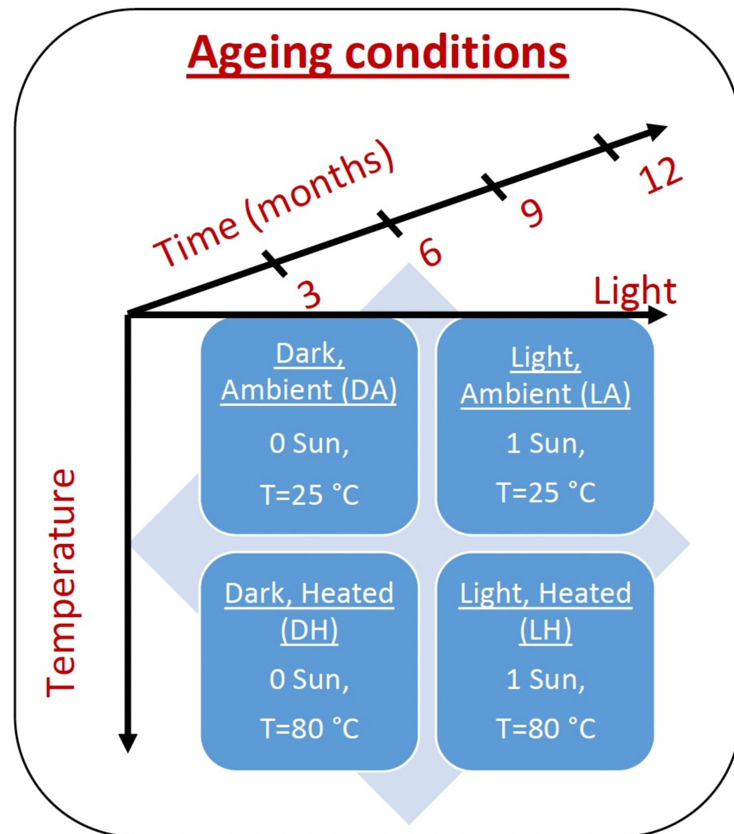

Experimental specifics

Bertoni, Manzoor (ASU):

* Double-side polished float zone (FZ) quality *n*-type c-Si wafers with (100) crystal orientation, 2.5 Ωcm resistivity and starting thickness of ~275 µm. These wafers went through rigorous cleaning procedure, during which they were cleaned in Piranha (H_2SO_4:H_2O_2|4:1) and RCA-b (H_2O:HCl:H_2O_2|6:1:1) solutions. For thinning the wafers, they were etched for variable time in an HNA (HF: HNO_3:CH_3COOH|10:73:17) mixture, ending with a dip in a buffered oxide (HF:H_2O|10:1) etch solution. Four different thicknesses were achieved in the range of 160–260 µm.

* These wafers were symmetrically passivated by depositing 50 nm of a-Si:H(i) on both sides using plasma enhanced chemical vapor deposition (PECVD) technique in Octopus I tool from INDEOtec SA.

* Effective minority carrier lifetime measurements at temperatures between 30–230 °C were performed with WCT-120TS tool from Sinton Instruments, where measurements were taken as temperature decreased from 230 °C. Data were collected in transient mode owing to the high lifetime of samples.

* The deposited a-Si:H(i) films were characterized with Fourier transform infrared spectroscopy (FTIR) technique using Nicolet 6700 spectrometer from Thermo Electron to determine the microstructure and hydrogen content of the films. Moreover, M2000 ellipsometer from JA Woollam was employed to characterize the thickness, bandgap (E_g), refractive index and lack of crystallinity in a-Si:H(i) film. Ellipsometric spectra were collected at multiple incident angles of 65, 70 and 75 degrees in reflection mode. Resulting spectra were fitted with a single Tauc-Lorentz oscillator and yielded a E_g of 1.68 eV.

Determination of defect density N(t)

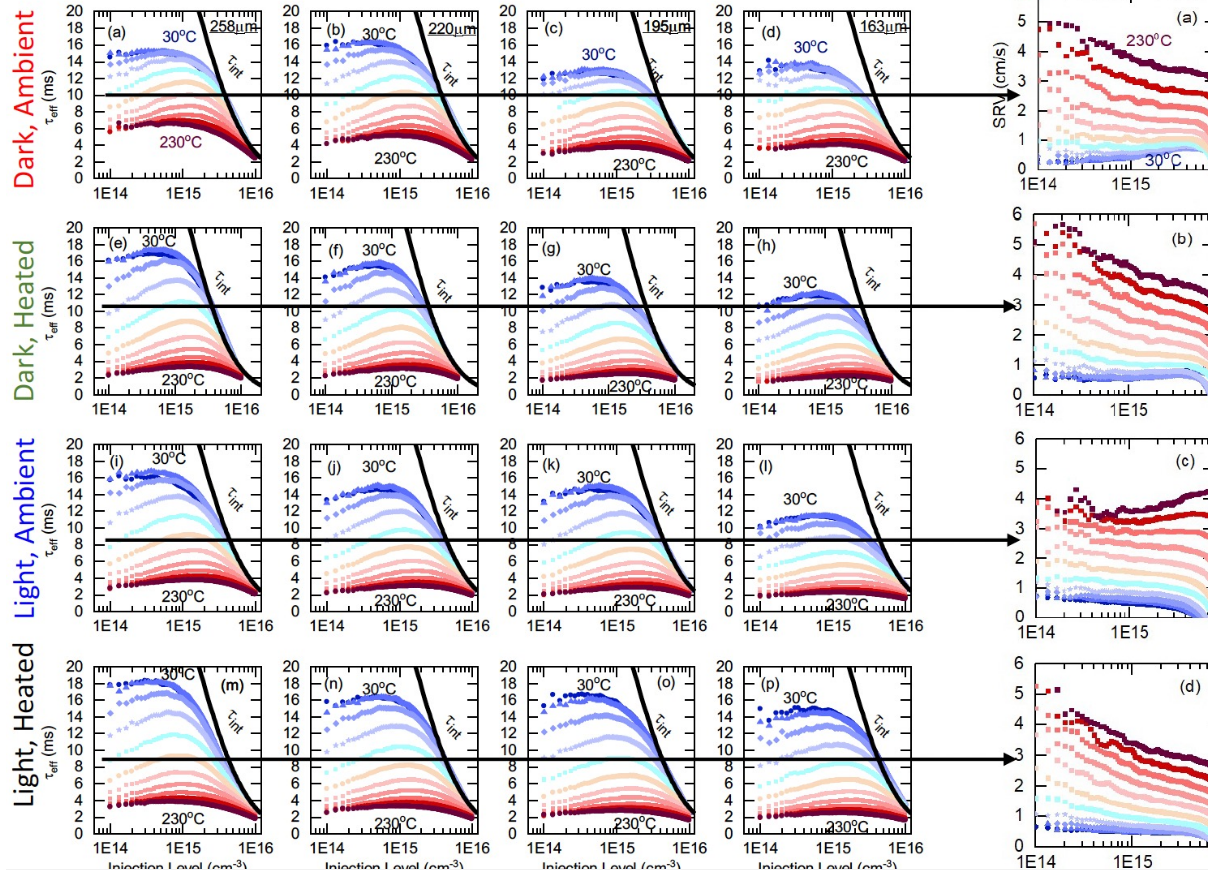

1. Determine SRV at each Δn from slope of $1/\tau_{eff}$ $(1/W)$
2. Repeat for every Δn for each T to obtain SRV(Δn, T)
3. Determine neutral interface defect density N_s by fitting SRV(Δn, T) at three values of Δn with the amphoteric defect model of Olibet, Baliff *et al.*

$$\frac{1}{\tau_{eff}} = \frac{1}{\tau_{aug}} + \frac{1}{\tau_{rad}} + \frac{1}{\tau_{SRH}} + \frac{2\times SRV}{W}$$

Interface Defect Density N(t) with Various Stressors

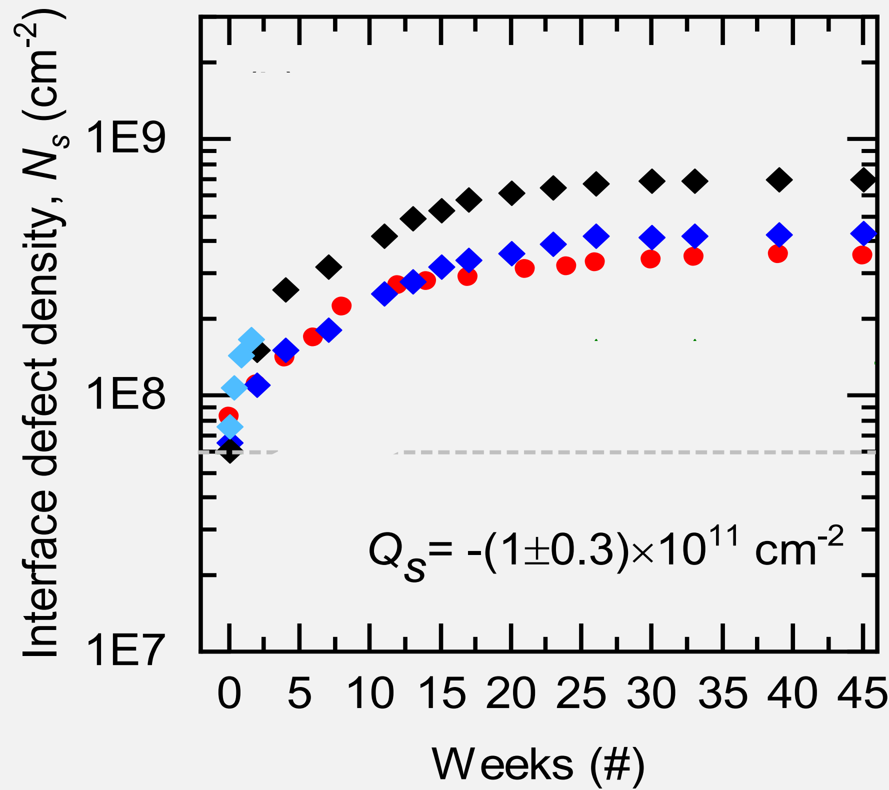

Dark ambient

Light ambient

Light heated

Previous expt.

$Q_s(t)$ was approximately constant

4. Repeat SolDeg for c-Si/a-Si:H with Si-H GAP

Created 60 c-Si/a-Si:H stacks
H content: 12%, 15%

Dominant dynamics:
H drifts away from interface

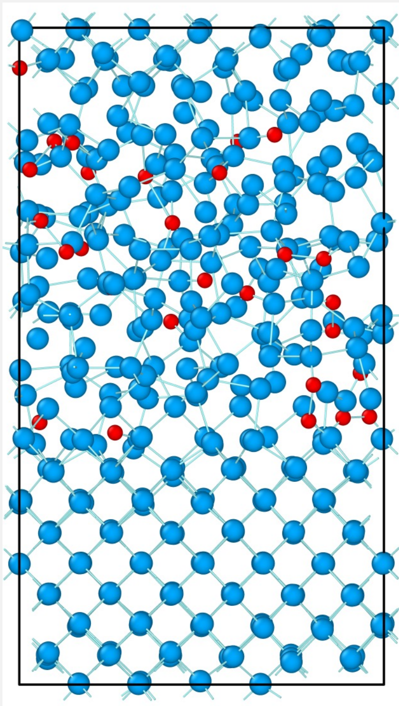

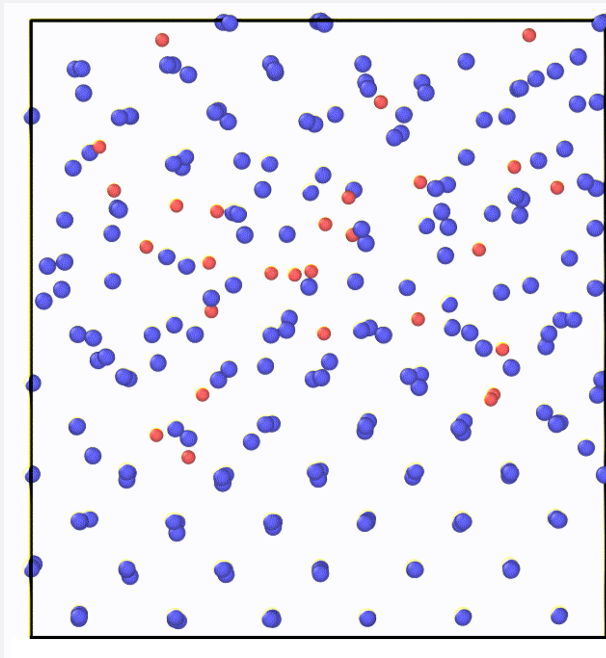

1. Movement of one H induced the collective motion of 10-20 atoms
2. We used the Inverse Participation Ratio IPR to verify that the H created a new dangling bond when it drifted away from the interface.
3. We verified that the dangling bond created a neutral defect

Why is hydrogen drifting? H energy exhibits a gradient

We measured the hydrogen energy at 25,000 locations

The hydrogen energy exhibits a gradient across interface This creates the force that drives H atoms away from interface

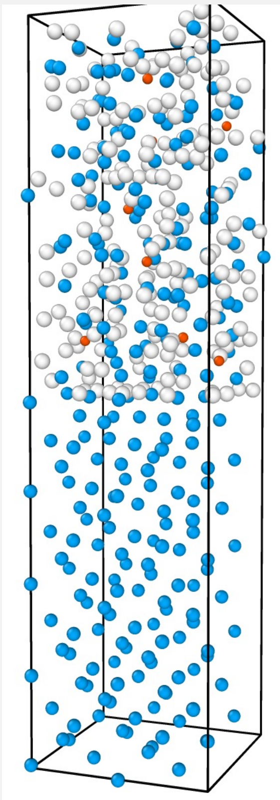

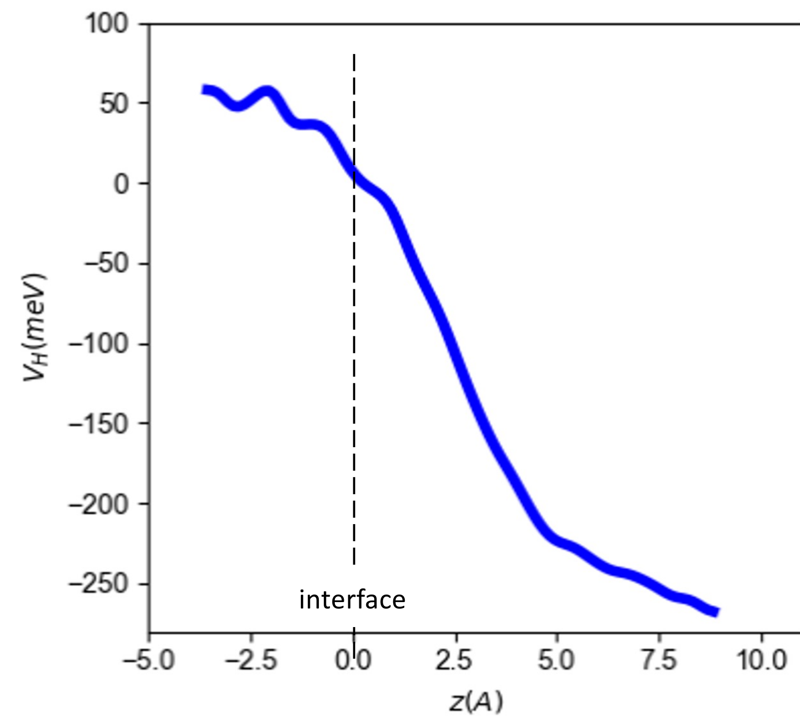

Energy barrier distributions of main processes

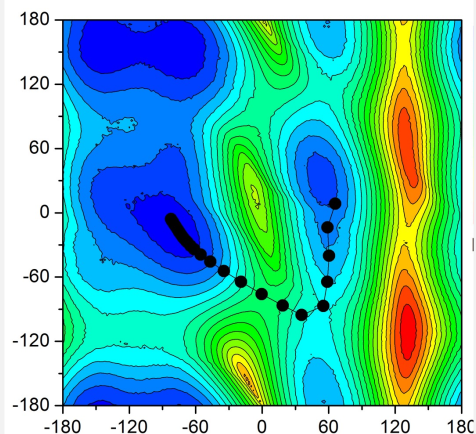

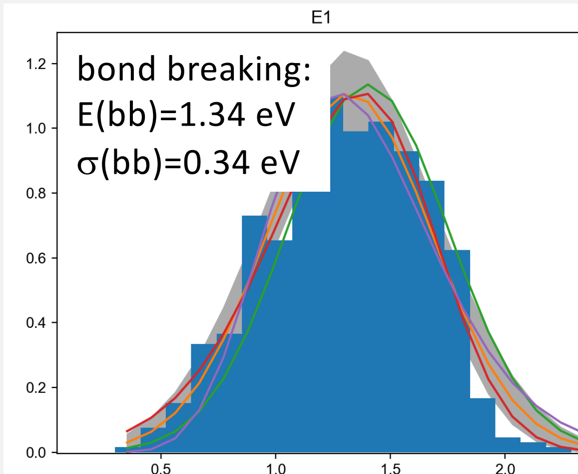

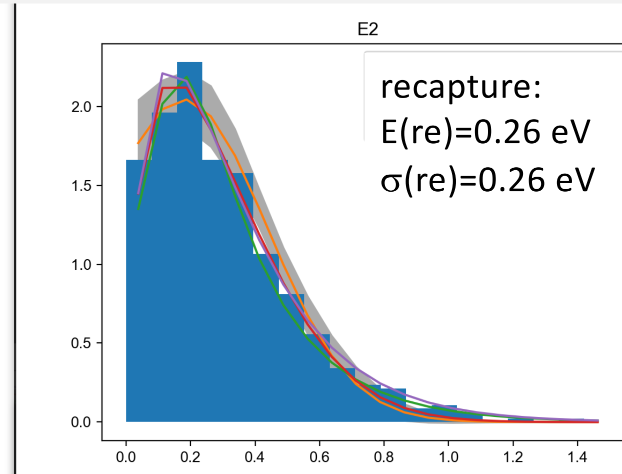

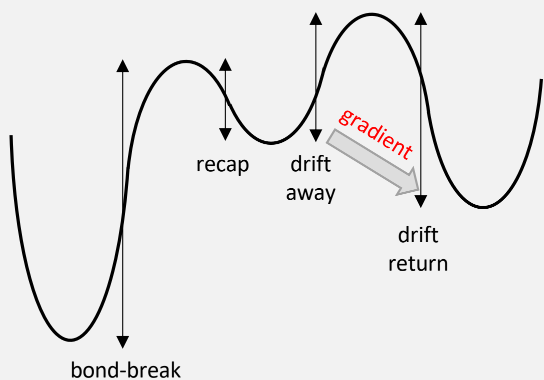

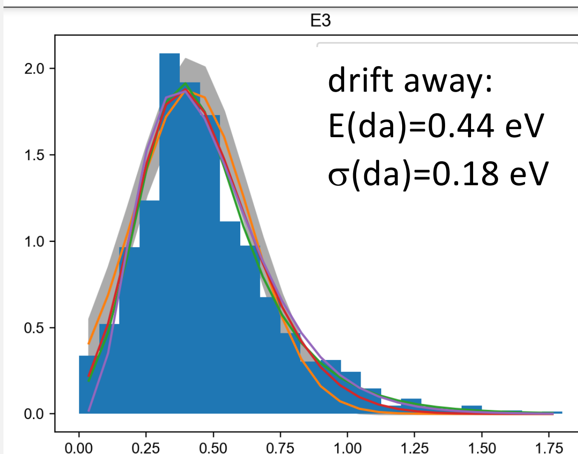

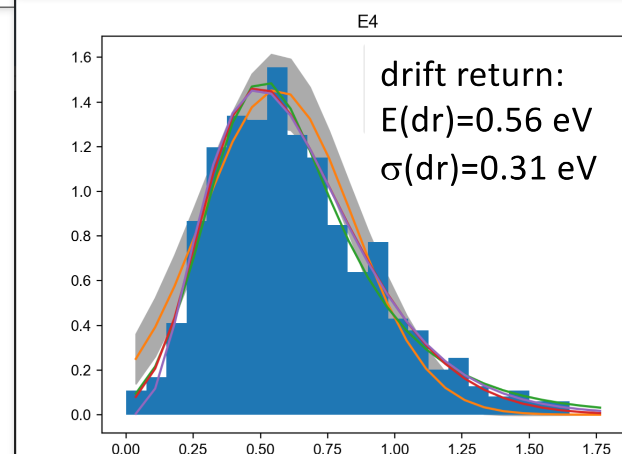

Novelty: Distributions from collective dynamics; H energy gradient

Matching up with previous work

	Si-H bond-breaking (eV)	Barrier to drift/ diffusion (eV)
This work	1.34	0.49
Santos et al. 1993	1.3	0.5
van de Walle 1994	1.2-1.5	0.5
Biswas 1998	1.4-1.5	0.48

Novelty:
Barrier energies are widely distributed: collective dynamics
Hydrogen energy has a gradient

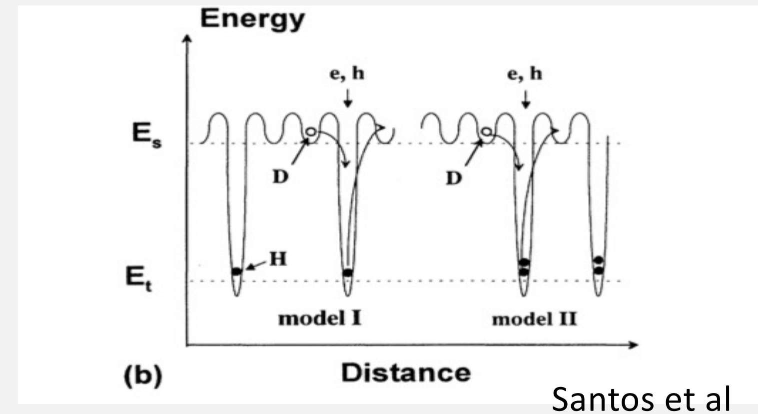

Santos et al

TABLE I. Parameters used in the simulations.

Parameter	Description	Model I
$C_H + C_D$	Total H+D density	7×10^{21} cm^{-3}
$E_m - E_s$	Shallow trap depth	0.5 eV
N_s	Maximum shallow trap density	1×10^{23} cm^{-3}
$E_m - E_t$	Deep trap depth	1.3 eV

Coupled dynamics across barriers: Analytic solution, SolDeg averaged

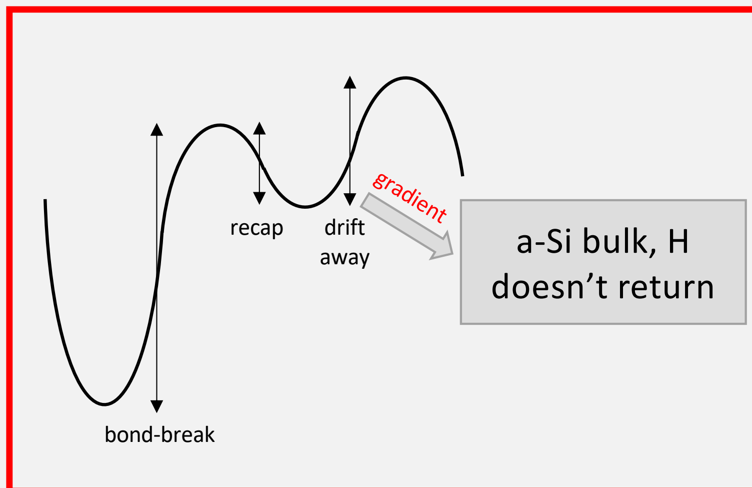

$$\frac{\partial}{\partial t}N_1 = -k_1 N_1 + k_2 N_2$$
$$\frac{\partial}{\partial t}N_2 = -k_2 N_2 - k_3 N_2 + k_1 N_1$$
$$\frac{\partial}{\partial t}N_3 = k_3 N_2$$

$$N_1(t) = N_0 e^{-\frac{\alpha t}{2}} \left(\cosh(\frac{\beta}{2}t) - \frac{k_1 - k_2 - k_3}{\beta}\sinh(\frac{\beta}{2}t)\right)$$

$$\alpha = k_1 + k_2 + k_3.$$

$$\beta \equiv \sqrt{\alpha^2 - 4k_1k_3}$$

1. The k_i rates are the thermal activation factors with the SolDeg-determined E_i energies of the barrier crossing processes.
2. Equations analytically solved for $N_i(t)$.
3. The $N_i(t)$ are averaged over the SolDeg-determined $P(E_i)$ distributions.

Defect generation with SolDeg-simulated energies reproduces data well

* Modelled N(t) with SolDeg-determined energies, averaged over SolDeg-determined distributions (line)
* Correspondence with experimental values (dots) is remarkable
* Not a fit – The six parameters are simulated, not fitted

N(t) from AS-KMC without analytics or model truncation validates three barriers model

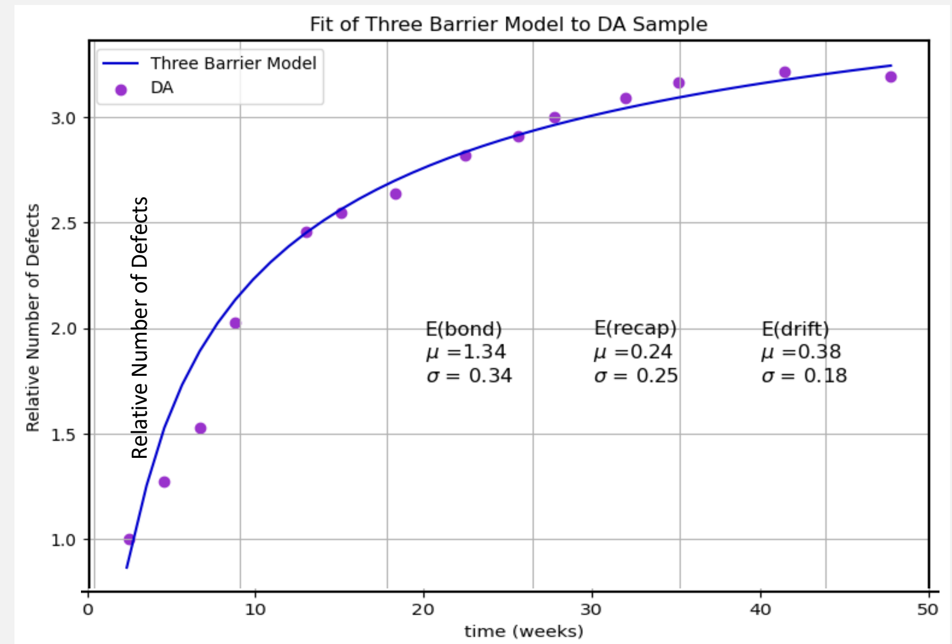

Defect generation with SolDeg-simulated energies reproduces data remarkably well

Broadened barrier distribution needed to provide active barriers

Degradation between 1 week and 1 year is driven by the barriers between 1.1 eV and 1.2 eV

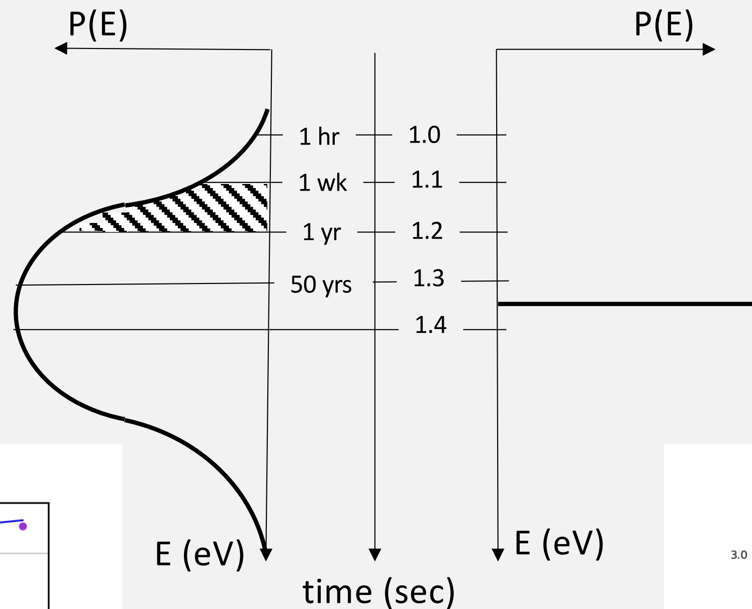

The 1.34 eV barriers are completely frozen between 1 week and 1 year. Broadening of P(E) around 1.34 eV provides barriers that are active in 1wk-1yr time window, and thus drive the time evolution of N(t).

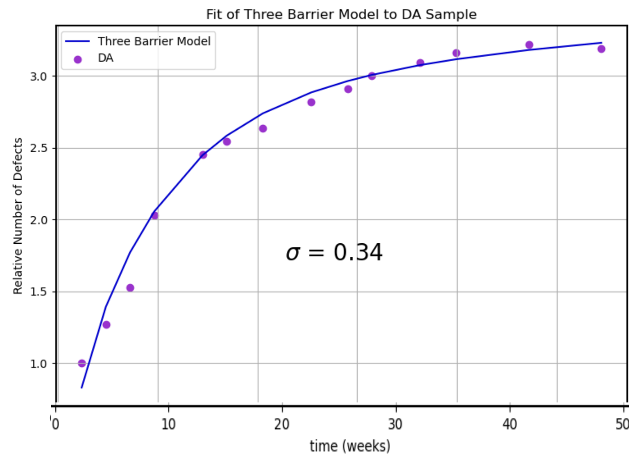

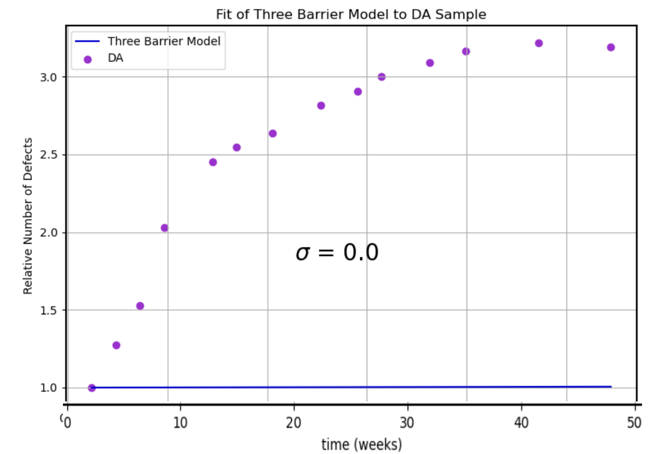

The impact of light on defect generation

How light impacts defect generation:
Photo-induced electrons, when localized at interface dangling bonds, modify the barriers of hydrogen drift.
Intuition: the recapture barrier will be impacted the most, as the captured photo-electron enhances the barrier against recapture

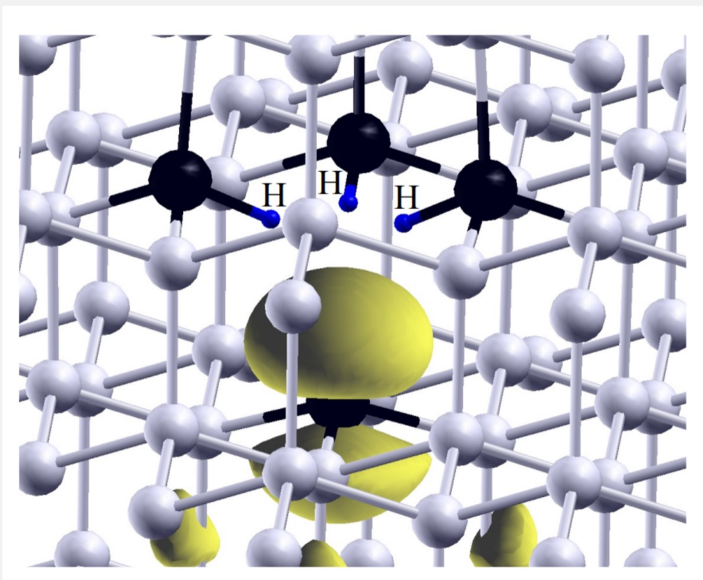

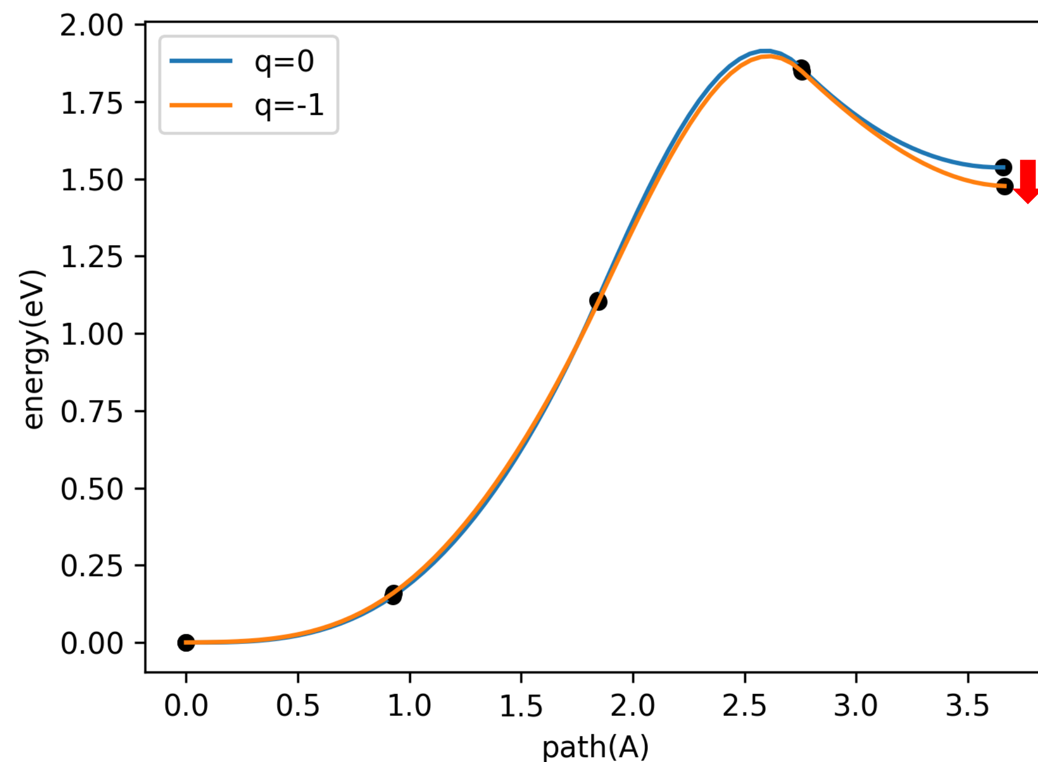

Δ bond-break:	-0.5%
Δ recapture:	+ 15%

Photo-induced electrons increase defect generation, moderately

We modified the bond-breaking and the recapture barriers accordingly in our Three Barrier Model, and recalculated the N(t) in the presence of light – shown with red line.

Our simulation results match the ASU data at long times - purple.

The majority of the defect generation is driven by thermal processes, not by light.

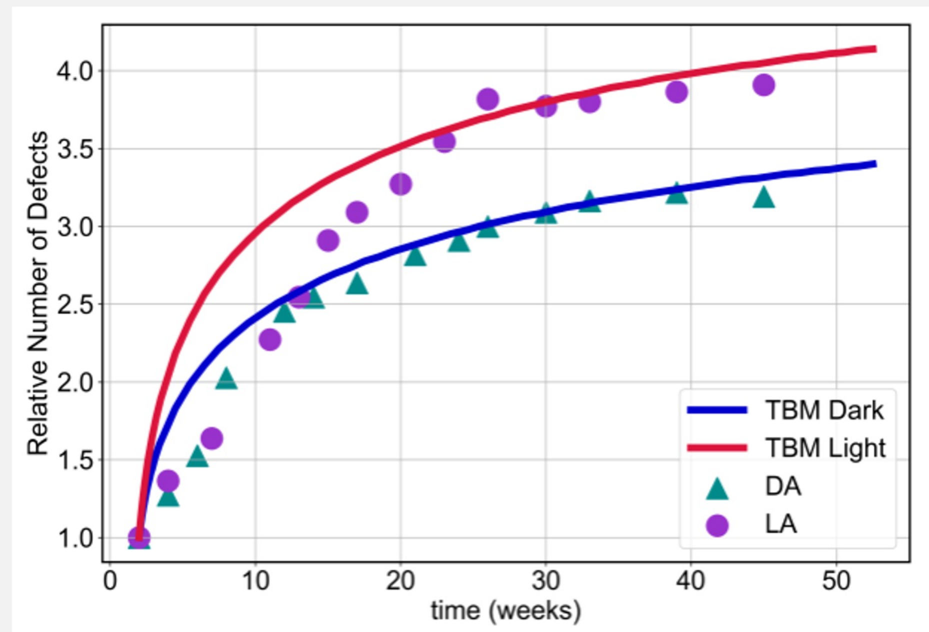

Light soaking studies at EPFL

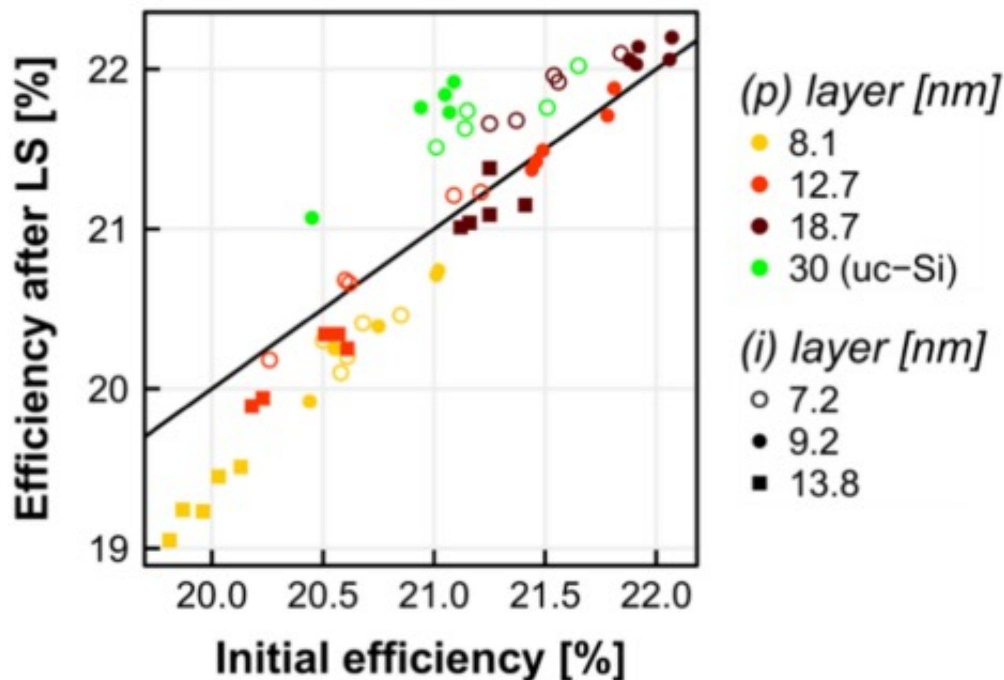

Cattin et al. (2021)

"In this work, we showed that, for well-optimized SHJ solar cells, light soaking treatment results in improved efficiency. However, this treatment can also cause degradation, e.g., when the (p) layer is **too thin** and exposed to light."

The ASU data did not show such LS effect at long times and ambient T. But its stacks did not have a doped layer or ITO, both of which effected the LS results.
(LS also may saturate? LS at higher T?)

We did observe the barriers that control H diffusion to be lowered by light. Maybe this helps H to diffuse to the interface and to increase passivation. This may be related to the observed Light Soaking enhancement.

Cause of H energy gradient? Si density gradient

Hydrogen energy gradient is in blue. -- Si density is in red.

The Si density gradient correlates with, and likely causes, the hydrogen energy gradient. The increasingly porous a-Si offers more room/lower energy spots for H.

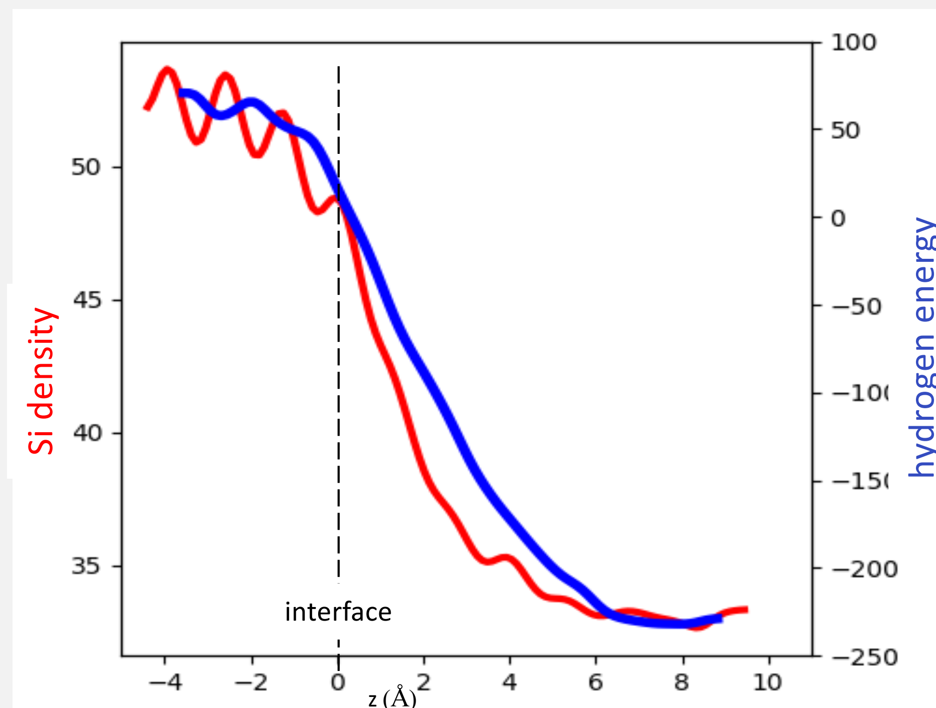

How to stop H-driven degradation? Reverse Si density gradient!

The H energy gradient was created by the Si density gradient. Idea: Reverse the H energy gradient by reversing the Si density gradient! This will create a density minimum at interface that traps the H and stabilizes the passivation.

We created 60 new c-Si/a-Si:H stacks where the Si density had a minimum at the interface. Again measured the H energy at 25,000 positions. Found that the H energy gradient has been changed into a minimum!

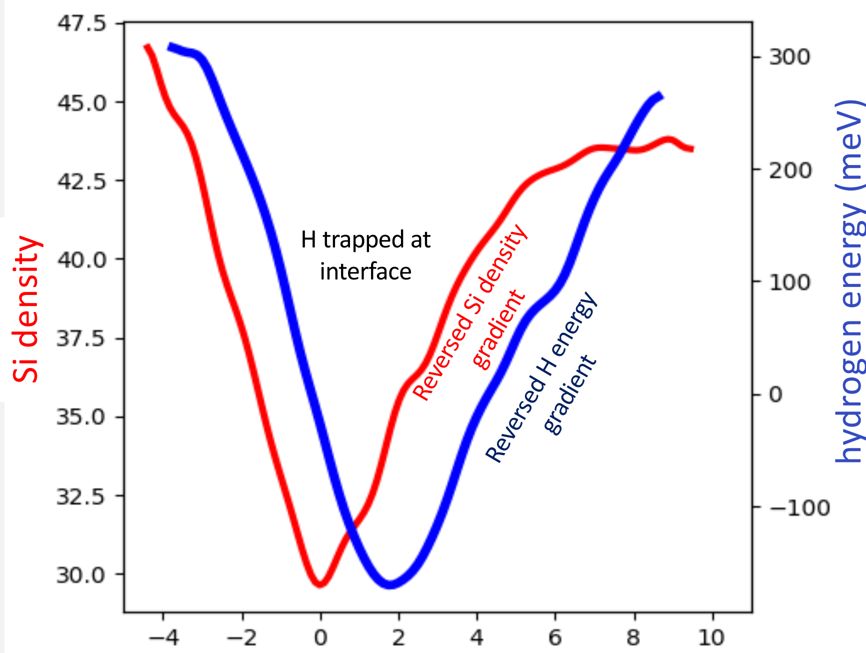

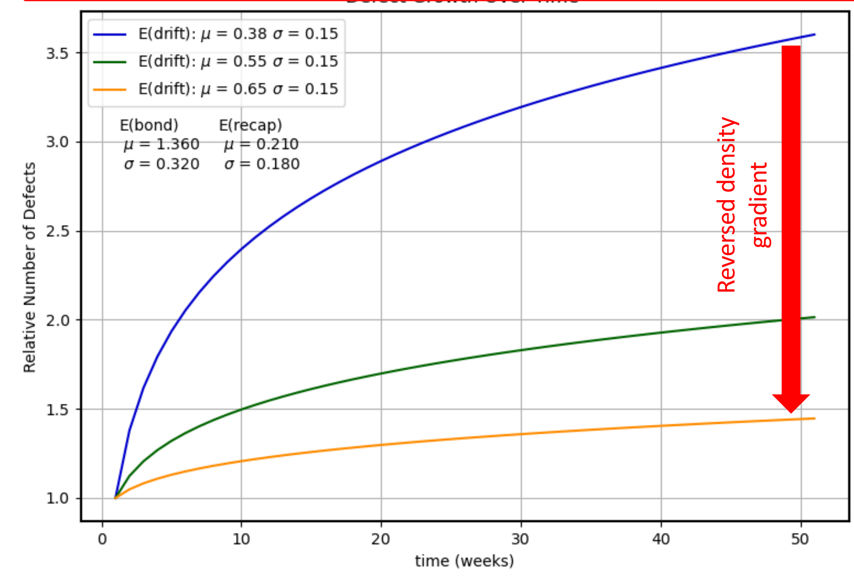

Bilayer adaptation of Reverse Si Gradient Improved Voc/Passivation

- Ru et al. Hanergy SolMat (2020): a-Si:H bilayer improved passivation
- Duan et al. Prog. in PV (2021): a-Si:H bilayer led to higher FF
- A. Smets et al. (2022): Increased Voc by 10 mV and efficiency by 0.6%
- Liu et al. J. Ap. Phys. (2016): Increased Voc by 5 mV
- Lee et al. ECS Solid State Lett.: (2014) Increased Voc by up to 25 mV

In our view, Voc was improved in these bilayer HJ cells because the degradation of Voc was suppressed from femtosec to the kilosec test times.

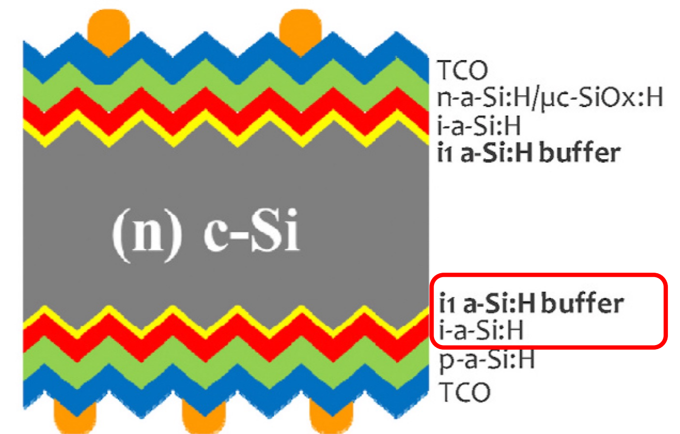

Trilayer Reversed Gradients started to appear in products in 2023

Huasun 04/2023

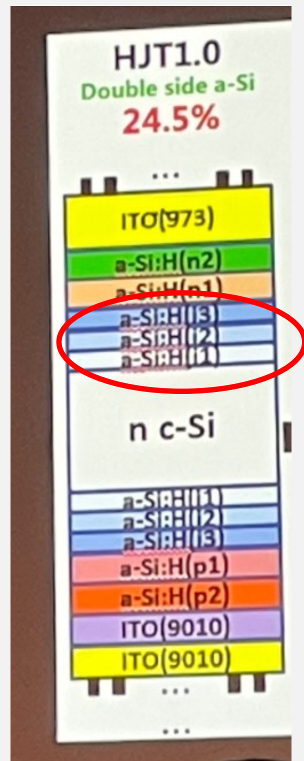

The multi-intrinsic a-Si:H layers

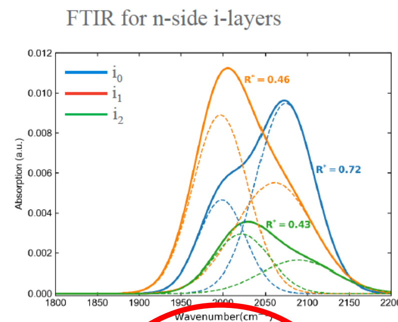

The averaged values

Layer	R*	C_H (%)
i_0	0.61	25.3
i_1	0.51	23.8
i_2	0.33	20.9

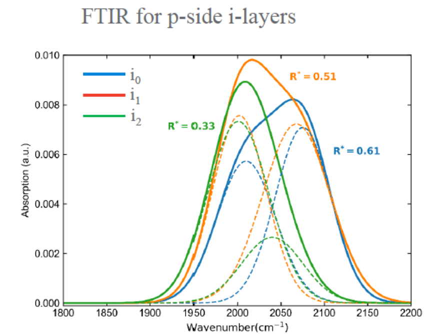

The averaged values

Layer	R*	C_H (%)
i_0	0.72	26.8
i_1	0.46	23.0
i_2	0.43	22.6

Meyer Burger as well

N(t) can be fitted with stretched exponential

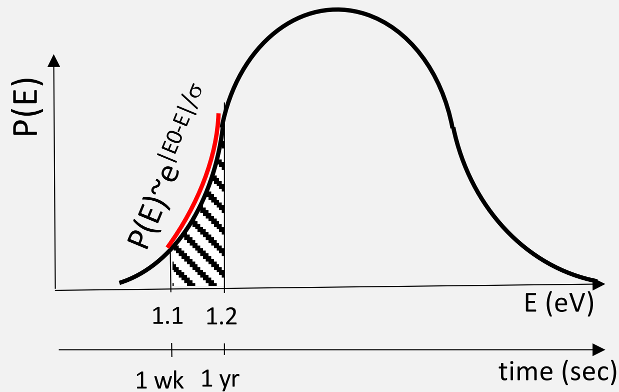

The 1 week-1 year time interval probes the P(E) barrier distribution only in the narrow range of 1.1-1.2eV. In this range P(E) can be well approximated with a simple exponential P(E)~e$^{|E0-E|/\sigma'}$.

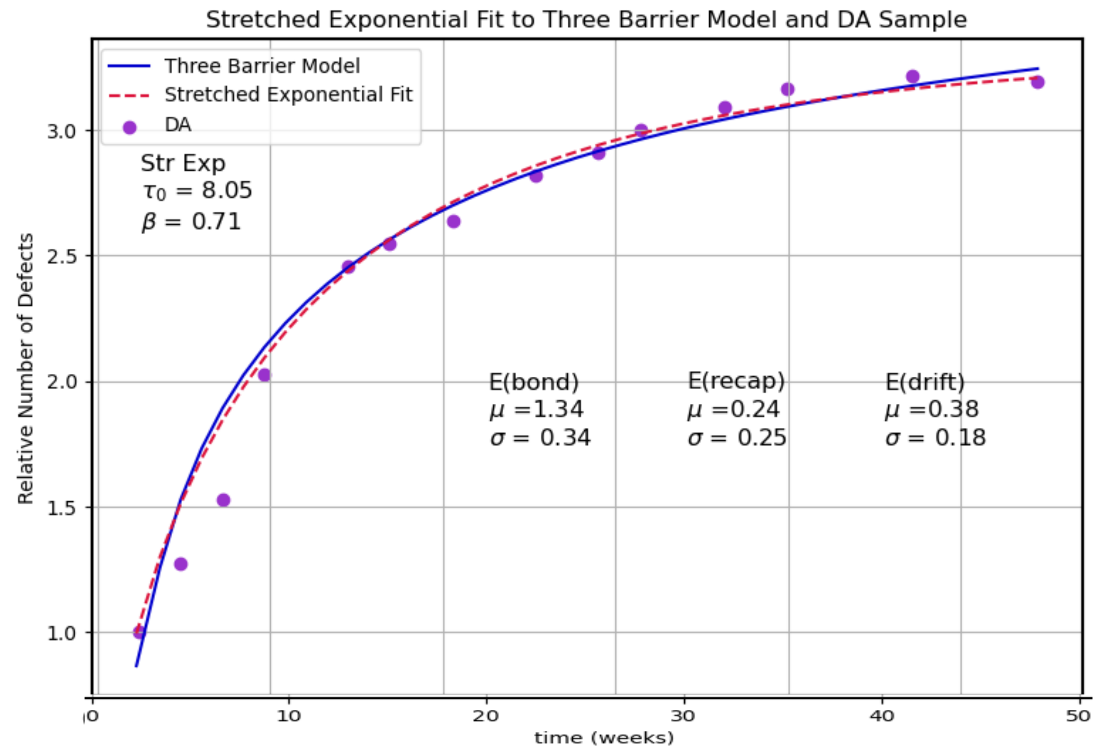

5. SolDeg analysis of TOPCon cells: Passivation is Sensitive to H

The excellent performance of TOPCon comes from the SiOx/poly-Si contacts providing excellent passivation, good carrier selectivity, and low contact resistance via the highly doped poly-Si.
But passivation is sensitive to temperature of fabrication.

Passivation is also sensitive to hydrogen. The recombination parameter J0 decreases up to an optimal H concentration, but increases for higher H concentrations.
Dynamics of passivation needs to be analyzed to optimize TOPCon cell performance.

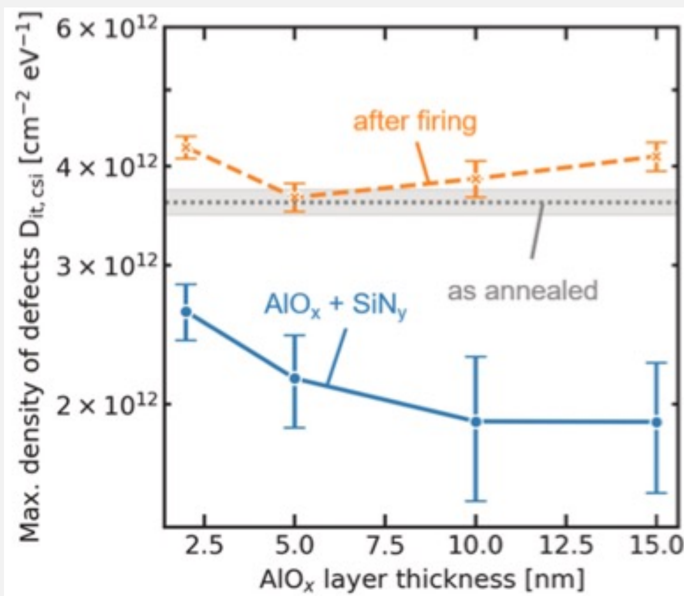

Hollemann *et al.* Sol. Energy Mater. Sol. Cell (2021)

AlOx is an H source

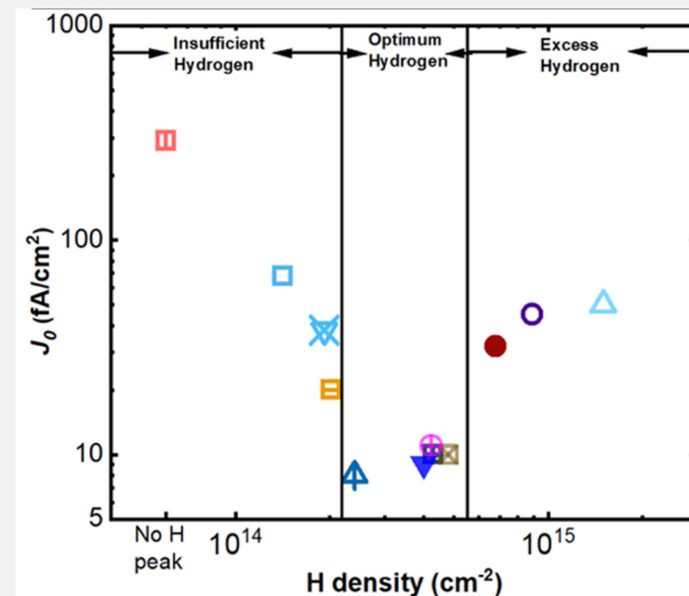

Kang *et al.* ACS Appl. Mater. Interfaces (2021)

Pinholes in TOPCon Cells

TOPCon cells use SiOx/poly-Si passivating contact.

SiOx layer thickness ~1.6 nm (POLO 2 nm)

The primary transport across insulating SiOx is quantum tunneling. An Ohmic contribution was also reported and attributed to pinholes in the SiOx.

A pinhole is a Si-rich region that partially or completely pierces through the SiOx resulting in unpassivated surface states and thus enhances recombination.

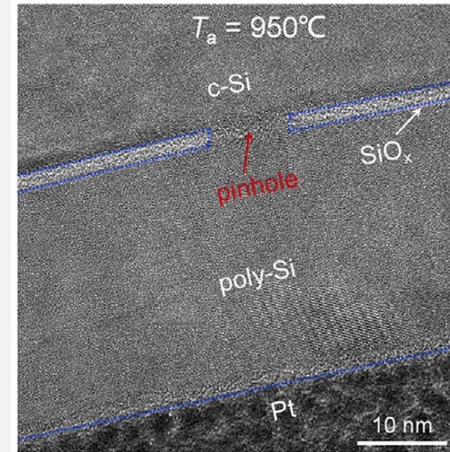

TEM image of pinhole in TOPCON cell.

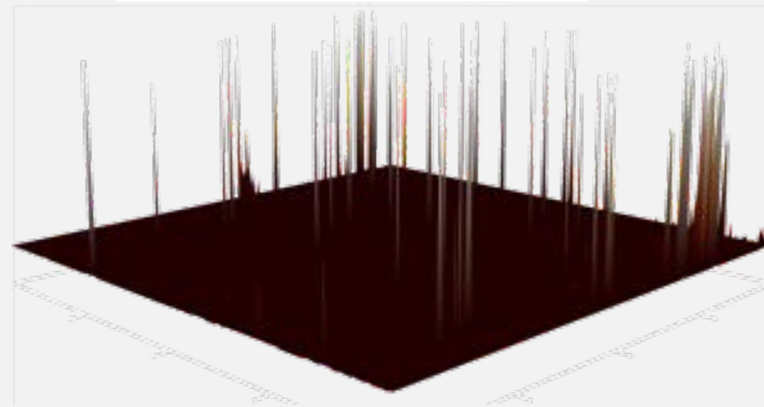

Current measured by STM in TOPCON cell.

Yang *et al.* *Cell Reports Physical Science* 2 2021 DOI: https://doi.org/10.1016/j.xcrp.2021

Proposed Driver of Pinhole Nucleation: Phase Separation of SiOx

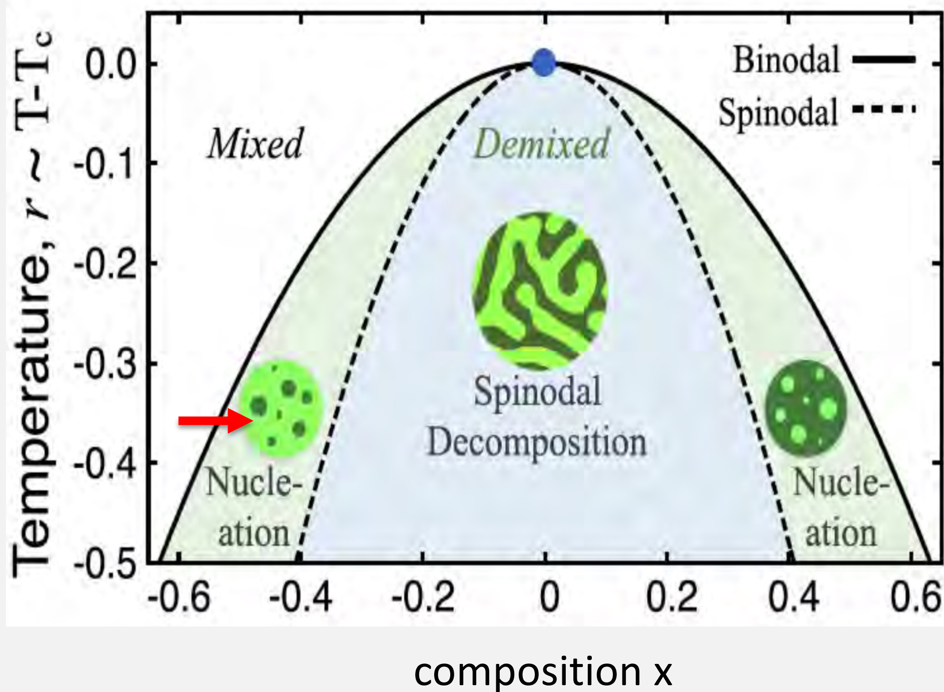

composition x

The SiOx layer is non-stoichiometric for x<2.
Non-stoichiometric compounds:
At higher T: Homogeneous mixed phase.
At lower T: Phase separation by minority phase nucleating in majority phase. -> Spinodal decomposition

Upon crossing the phase separation line (solid) from the homogeneous phase, the free energy of SiO_x is lowered by stoichiometric Si bubbles/pinholes nucleating within a background that evolves towards stoichiometric SiO_2. The nucleation is controlled by barriers.

Adapting SolDeg for the Simulation of Fabrication of TOPCon Cells

To simulate the thermal stress of the firing process, TOPCon cells (stacks) were formed with a c-Si wafer and a 1.6 nm SiO_x layer on top; x ~ 1.6-1.8.

The periodic boundary conditions provided a structure consistent to c-Si/SiO_x/poly-Si.

Stacks were heated to temperatures ~1500 ^{0}C, followed by a quench back down to 25 ^{0}C.

All Simulations were performed using the LAMMPS molecular dynamics simulator, with the ReaxFF developed for simulating c-Si/SiO_2 interface [1].

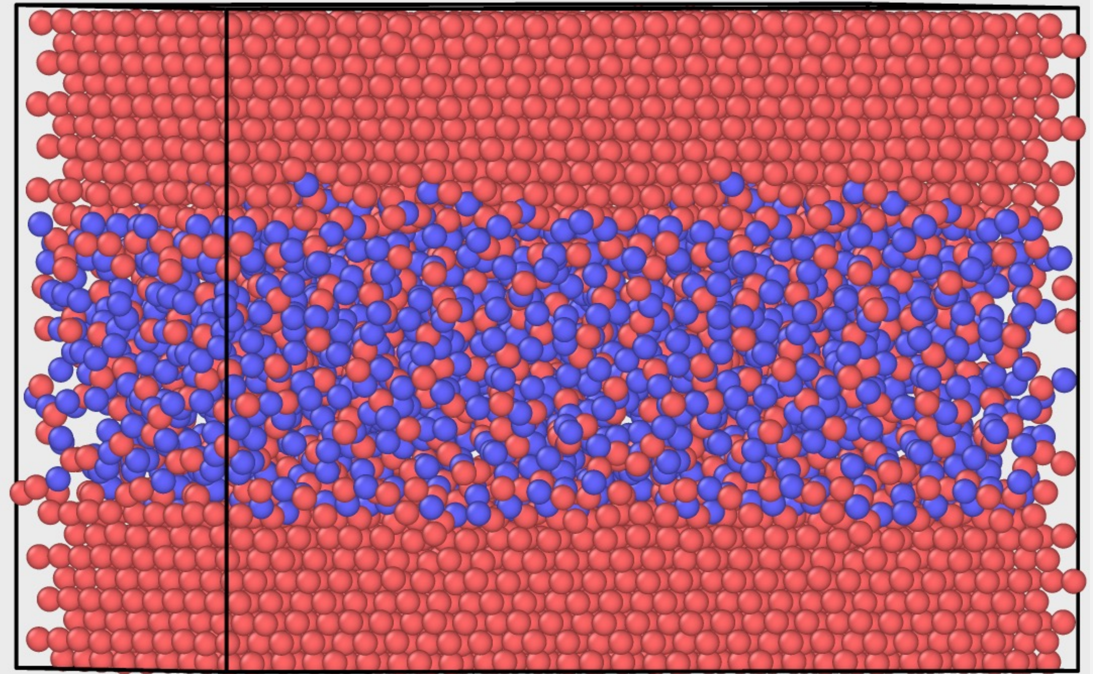

Si-Red, O-Blue

1. Nayir, N. van Duin, A. and Erkoc, S. *J. Phys. Chem. A* (2019)

Pinhole Formation is Driven by Nucleation

The results of our TOPCon firing simulations clearly show that pinholes form via nucleated phase separation.

Temperature of 1500 ^{0}C, above representative values. Top view:

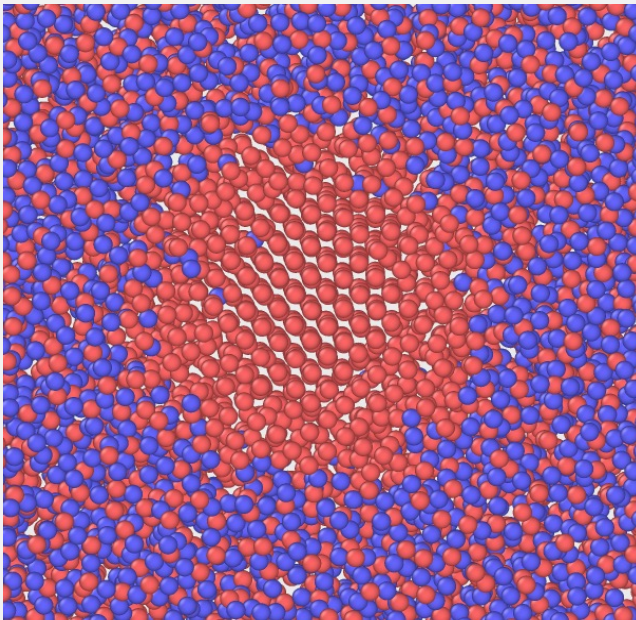

SiO_x

c-Si

SiO_x

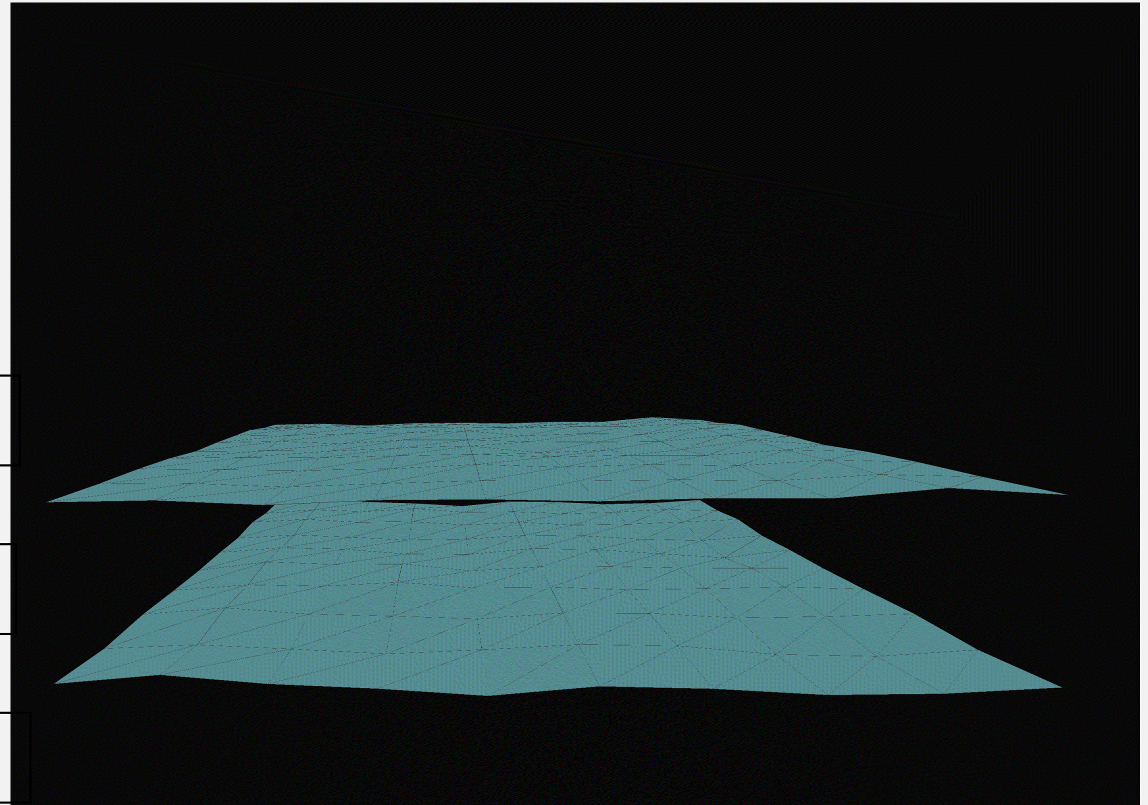

Sideview of the evolution of iso-surface surrounding the $x < 0.5$ volume in our simulations.

Simulation of the Effects of Hydrogen

Using our initial structures we added hydrogen in various concentrations, $1.4\times10^{14} - 2.5\times10^{15} cm^{-2}$ average areal density.

Stacks were heated to fabrication-realistic lower temperatures between 700 ^{0}C-1300 ^{0}C, followed by quenching back to 25 ^{0}C.

The simulation showed distinct regimes for low, [H]<4 $\times10^{14} cm^{-2}$, and high [H]>$4\times10^{14} cm^{-2}$ concentrations of hydrogen.

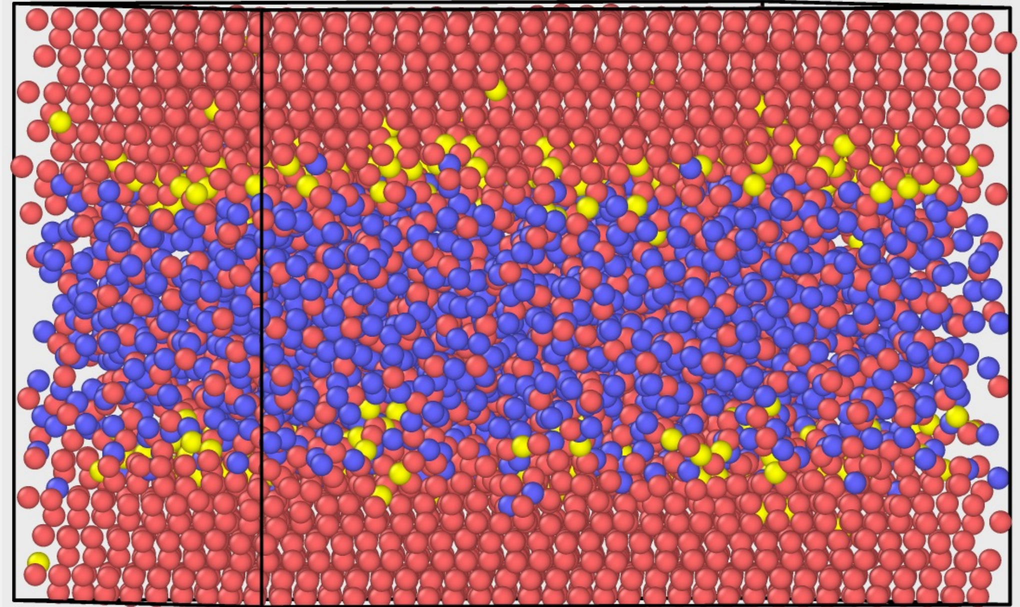

low [H]<$4\times10^{14} cm^{-2}$
Si-Red, O-Blue and H-Yellow.

Low [H] Regime – Hydrogen Passivates Interface

At low [H], $< 4\times10^{14} cm^{-2}$, hydrogen migrates to the interface, passivates the Si dangling bonds and relaxes the strained bonds. No pinholes formed during the representative simulation time.

At low [H] the density of interface Si dangling bonds (DB) decreases with increasing [H]

(These dangling bonds are consistent with the known P_{b0} defects)

The total number of strained bonds is large, thus we find that ideal passivation requires [H] >> DB

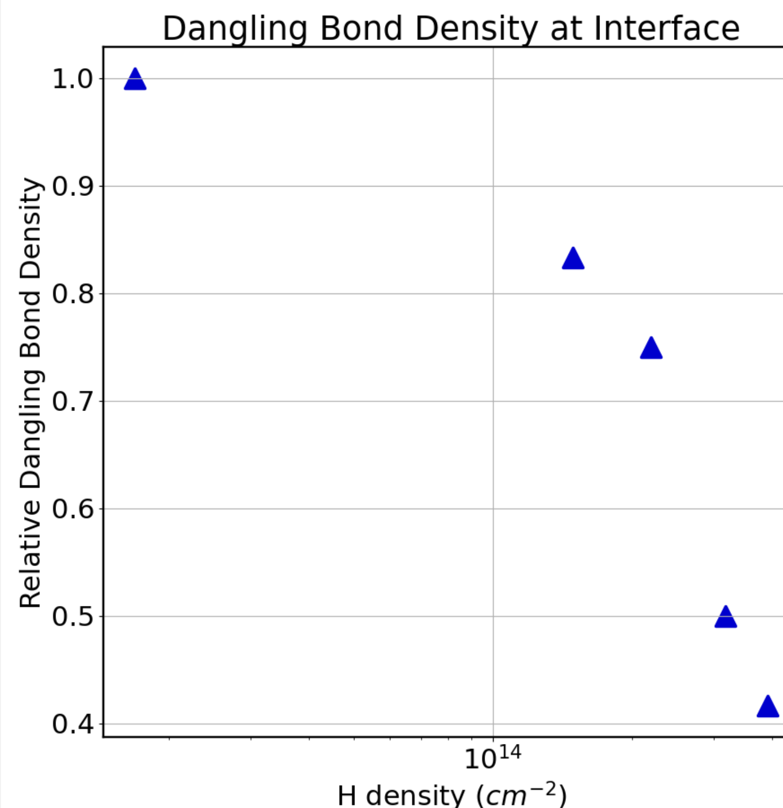

High [H] Regime – Hydrogen Induces Nucleation of Pinholes

At high [H], > $4{\times}10^{14} cm^{-2}$, the interface region becomes saturated, and a significant concentration of H remained within the SiOx layer. H in the bulk SiOx layer primarily resides in bond center configurations. We observed extensive pinhole formation

The addition of hydrogen changed the competing terms in the free energy of the system. Hydrogen lowered the energy of the phase separated configuration.

For SiOx layers that did not support pinhole formation, the addition of sufficient amount of H drove the SiOx layer across the binodal line and nucleated pinhole formation.

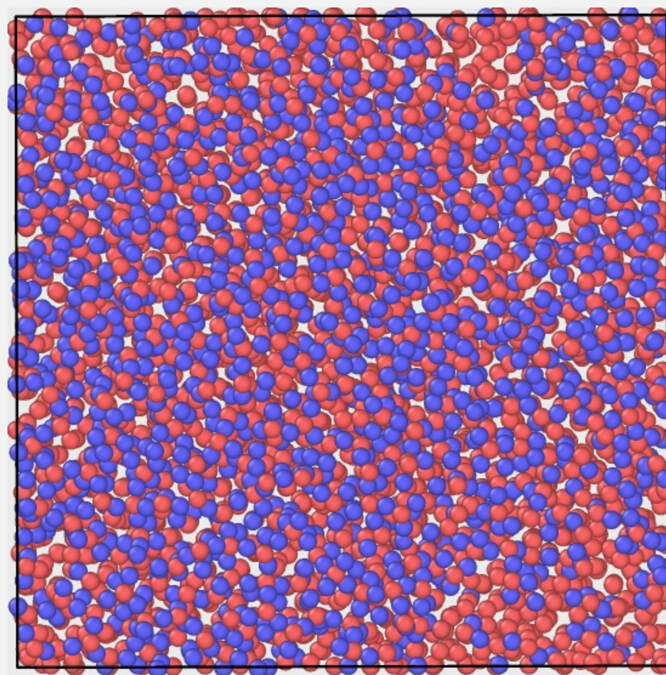

Simulated firing with [H] = 0

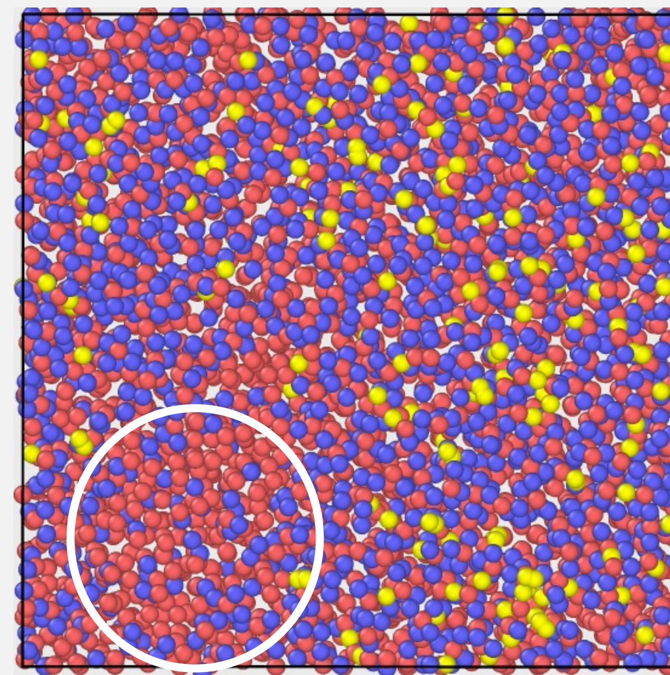

Simulated firing with [H] = $1.2{\times}10^{15} cm^{-2}$

High [H] Regime – Hydrogen Induces Nucleation of Pinholes

At high [H], > $4{\times}10^{14}cm^{-2}$, the interface region becomes saturated, and a significant concentration of H remained within the SiOx layer. H in the bulk SiOx layer primarily resides in bond center configurations. We observed extensive pinhole formation

The addition of hydrogen changed the competing terms in the free energy of the system. Hydrogen lowered the energy of the phase separated configuration.

For SiOx layers that did not support pinhole formation, the addition of sufficient amount of H drove the SiOx layer across the binodal line and nucleated pinhole formation.

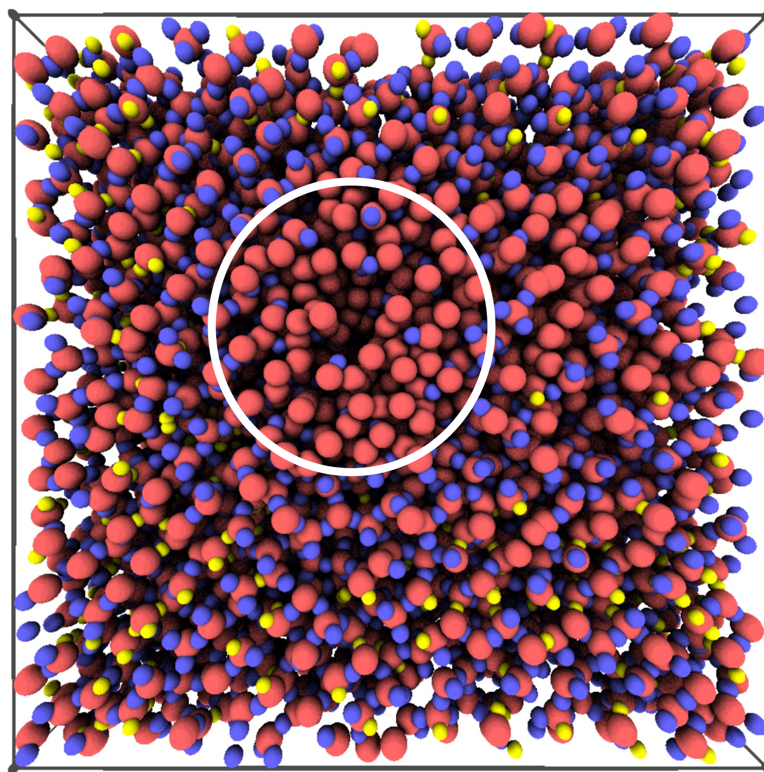

Nucleation is driven by H shifting balance of competing energy terms

The nucleation energy barrier barely changes as [H] grows from 3X10^{12} cm^{-2} to 3X10^{14} cm^{-2}, but once it exceeded 3.6x10^{14} cm^{-2}, the barrier rapidly decreased as [H] approached 1X10^{15} cm^{-2}.

$$\Delta F = [NF_{Si} + (N_0 - N)F_{SiO2}] + \sigma N^{2/3} - N_0 F_{SiOx} =$$

$$= const. - [F_{SiO2} - F_{Si}]N + \sigma N^{2/3}$$

energy of pinhole surface

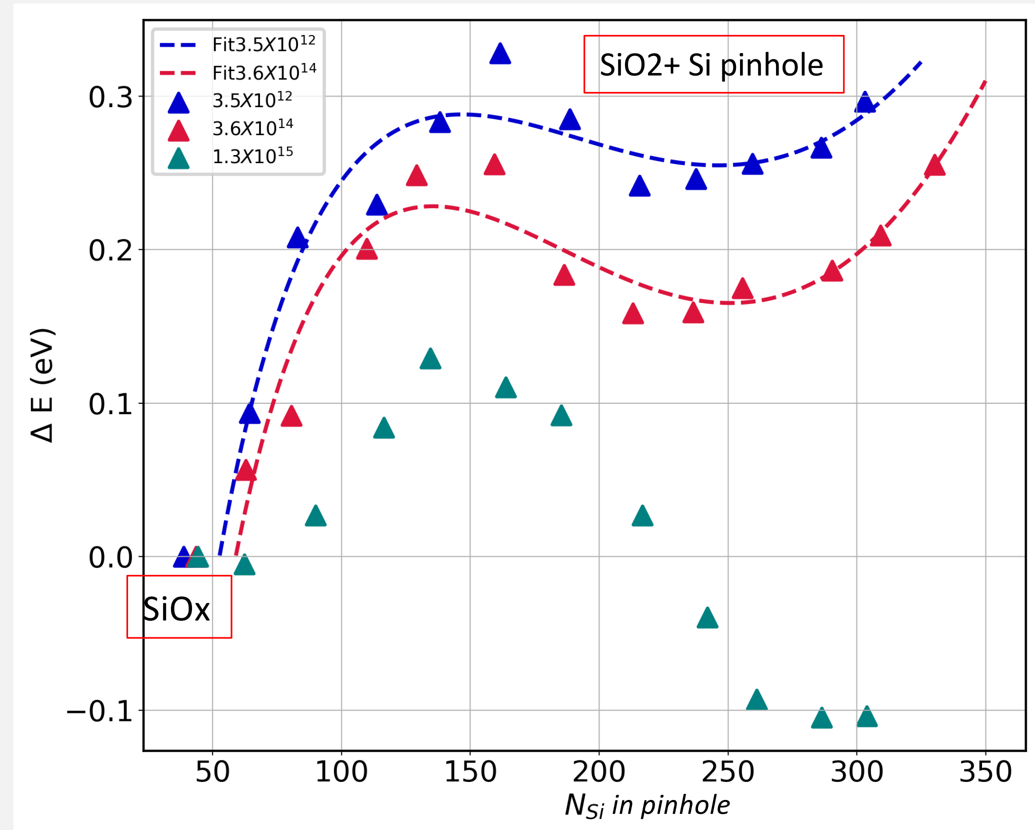

Hydrogen Induced Pinhole Nucleation

High [H] lowers the nucleation barrier of pinholes.

[H] < $4{\times}10^{14} cm^{-2}$ pinholes did not form within the timeframe of the simulation.

[H] > $4{\times}10^{14} cm^{-2}$ pinholes did form.

At higher [H] pinholes form faster.

Pinhole formation rate as a function of [H] for pinholes within simulation timeframe.

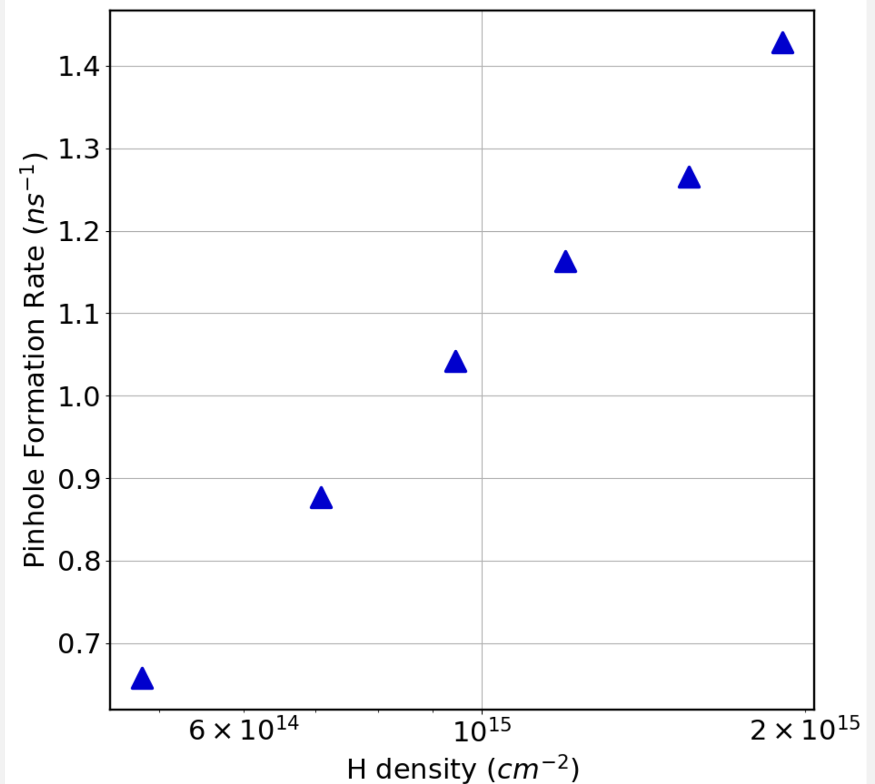

Pinhole Nucleation is a Consistent Theory of Recombination Minimum

Kang *et al.* ACS Appl. Mater. Int. (2021)

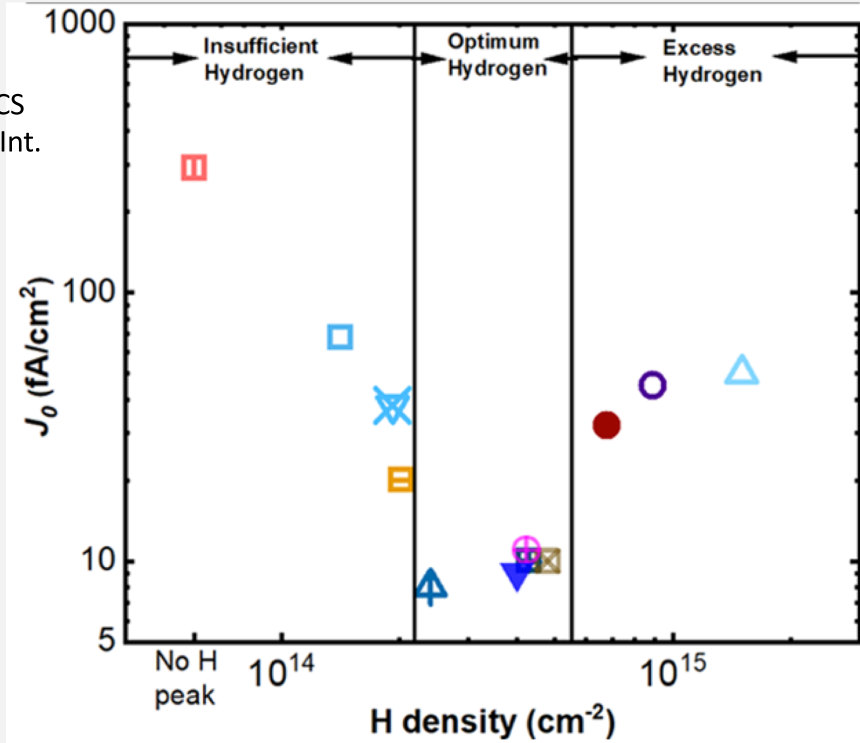

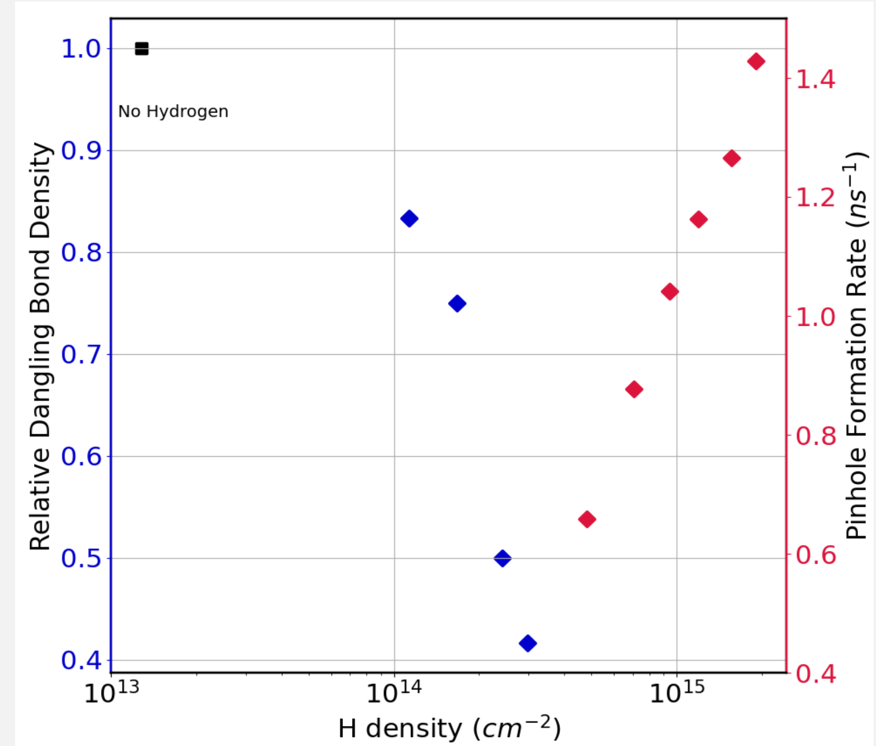

At low [H], hydrogen increasingly passivates dangling bonds at the interface.

At high [H], H induces nucleation of pinholes that act as recombination centers at the c-Si interface.

Hydrogen Induced Nucleation of Pinholes is Reversible

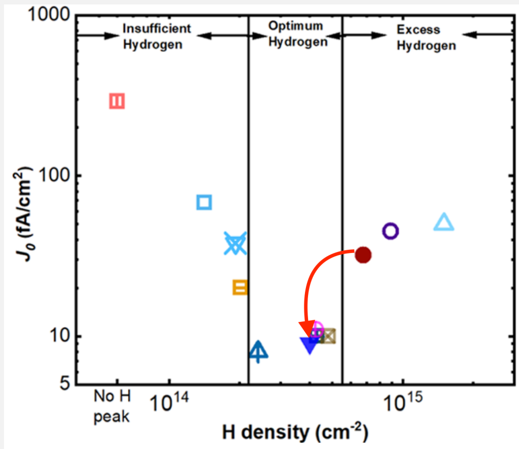

Kang *et al.* reported that upon extracting H by N_2 annealing at high [H], they could lower J_0.
In our theory, pinhole formation is the consequence of SiOx being driven across the binodal line by adding H. In this picture, subsequent removal of H drives the system back across the line. This makes pinhole formation energetically unfavorable and dissolves the pinholes.

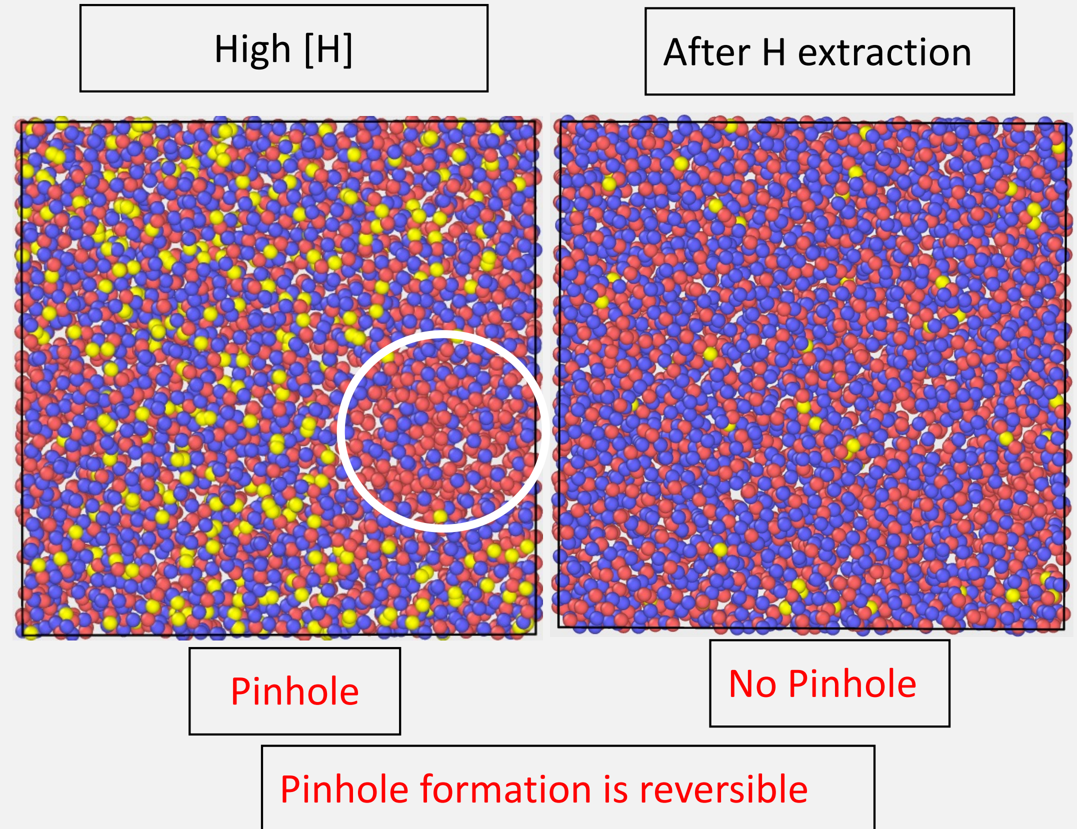

Predicting Electronic Defects from Structural Info by Machine Learning

DFT is much slower and computer intensive than Molecular Dynamics (MD) that is used for Structural Simulations

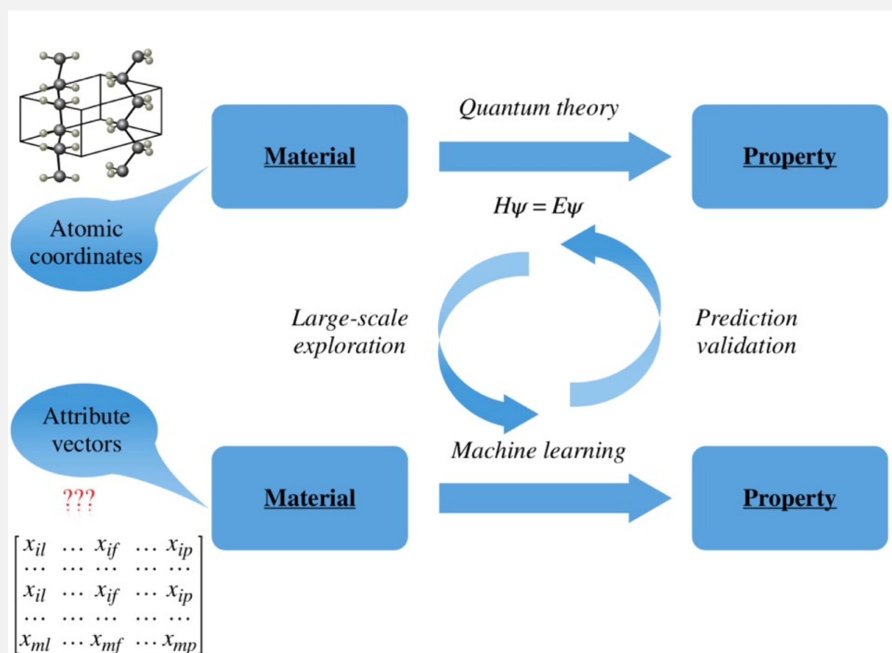

	Training/validation accuracy		
	cSi	cSi/aSi	cSi/aSi:H
Bond lengths only	68%/68%	61%/61%	60%/60%
3-body angles only	97%/94%	85%/78%	77%/77%
Bond lengths + subset of 3-body angles	98%/95%	75%/75%	76%/76%
Bond lengths + 3-body angles	98%/97%	90%/81%	78%/78%
Bond lengths + 3-body angles + 4-body angles	99%/97%	93%/83%	80%/78%

We ML-trained algorithms on cSi; cSi/aSi interfaces; and cSi/aSi:H structures to find electronic defects
We achieved 78%-97% accuracy to predict quantum electronic defect properties from structural info alone

SUMMARY

1. Developed SolDeg platform to analyze defect dynamics over 24 orders of magnitude in time

2. For Heterojunction cells, developed scaling law of accelerated testing: $t(norm) \sim t(acc)^{(T(acc)/T(norm))}$

3. Developed Machine-Learning-based Si-H GAP potential for most accurate Molecular Dynamics simulation of c-Si/a-Si:H heterojunctions

4. Reported experimental analysis: Degradation is driven by neutral defect generation at interface

5. SolDeg-simulated defect generation was remarkably consistent with experiments

6. SolDeg: H drift from interface causes degradation. Proposed Reverse Si Density Gradient to suppress Voc degradation from 0.5 %/yr to 0.1%/yr. This also increases Voc by 10-15 mV

7. SolDeg modelled TOPCon passivation dynamics:

low [H]: interface passivation lowers recombination

high [H]: induces nucleation of pinholes that increase recombination

passivation can be optimized by well-chosen hydrogen concentration

ACS App. Mat. & Interfaces p. 32424 (2021)
Phys. Rev. Mat. 6, 065603 (2022)
Nature Comm. Mat. /doi.org/10.1038/s43246-023-00347-6 (2023)
TOPCon: submitted

Team members

Davis Unruh
UCD – Samsung

Reza Vatan
ASU-First Solar

Andrew Diggs
UCD

Salman Manzoor
ASU-First Solar

He is handsome too

Zitong Zhao
UCD

Stephen Goodnick
ASU

Mariana Bertoni
ASU

Gabor Csanyi
Cambridge, UK

THANK YOU